FORCED CONVECTIVE HEAT TRANSFER TO COOLED CYLINDERS AT LOW REYNOLDS NUMBERS AND WITH LARGE TEMPERATURE DIFFERENCE

by

A.M. Ahmed

T.N.67-5

Mechanical Engineering Research Laboratories

McGill University

This work was performed under contract to Canadian Armament Research and Development Establishment, Val Cartier, Quebec, and was supported partly by D.R.B. Grant 9550-06.

Montreal

September, 1967.

For the purpose of determining a general correlation for forced convective heat transfer coefficient for circular cylinders in cross-flow under conditions pertaining to cooled-film application for measurements in flames and hypersonic wakes, heat transfer measurements were obtained under simulated conditions created in a plasma-jet. Measurements were made by means of constant temperature, internally cooled, cylindrical film sensors in the Reynolds number range 4 - 75, for various temperature loadings, the maximum being $T_\infty/T_s = 4$, and for flows composed of He, N_2 and CO_2 and their mixtures. The plasma-jet conditions were maintained such that at the points of measurements, i.e. at the potential core of the jet, ionization was negligible, recombination was complete and the turbulence intensity was low. By a statistical analysis, the data obtained for $Re_M = 4$ to 40 were correlated by,

$$Nu_M \left(\frac{\nu_\infty}{\nu_M}\right)^{.15} = .2068 + .4966\, Re_M^{.45}$$

All the fluid property values in the dimensionless parameters are evaluated at the arithmatic mean temperature. A kinematic viscosity ratio instead of the more usual temperature ratio was considered in the temperature loading factor to account for the different dependency of the transport properties on temperature for different gas species.

Even though no previous correlations were obtained for conditions considered here, the direction of the temperature loading effect and the departure from King's law appear to be consistent with some of the existing correlations.

NOMENCLATURE

ROMAN SYMBOLS

A	Constant
a	Surface area of the cylinder (sensor)
B	Constant
C	Constant
C_p	Specific heat
d	Diameter, sensor
G	Mass velocity
h	Heat transfer coefficient
K	Thermal conductivity
M, m'	Constants
N, n'	
Nu	Nusselt number $\frac{hd}{K}$
Pr	Prandtl number $\frac{c_p \mu}{K}$
Q	Heat transferred
R	Resistance, electrical
Re	Reynolds number $\frac{Vd\rho}{\mu}$, $\frac{Vd}{\nu}$
T	Temperature
V	Mean flow velocity normal to cylinder (sensor)

GREEK SYMBOLS

α	Temperature coefficient of resistance
μ	Absolute viscosity
ν	Kinematic viscosity
ρ	Mass density

SUBSCRIPTS

M	Arithmatic mean and when referring to dimensionless groups signifies that the fluid property values are evaluated at the arithmatic mean temperature, i.e. at $(Ts + T_\infty)/2$
S	Surface, sensor
∞	Free stream

I. INTRODUCTION

I. 1. Direct measurement of dynamic characteristics in high temperature flow fields as exist in laminar and turbulent flames, hypersonic wakes, rocket nozzle flows, demand a rapid response instrument able to withstand high temperature environments. An extension of constant-temperature hot wire anemometry to constant-temperature, internally cooled, thin-film anemometry towards this end is considered. (Compared to hot-wire sensors, cooling of the cylindrical film sensor not only prevents melting of the sensing element but also allows interpretable measurements to be obtained when the environment is at a higher temperature than the sensing film, without sacrificing response.) The principle of operation of the cooled-film sensor as compared to that of the hot-wire or hot-film sensors is shown in Fig. 1. For cooled film operation when the environment temperature is greater than the sensor temperature, a heat balance applied to the sensing film gives: (see Fig. 1)

$$Q_{ENV} = Q_{COOLANT} - Q_{SUPPLIED} \quad \ldots\ldots \quad 1\,A$$

In the above relation $Q_{SUPPLIED}$ is the heat equivalent of the electrical power supplied by an analog network to maintain the constant film temperature T_S. Q_{ENV} is the heat absorbed by the film from the environment and $Q_{COOLANT}$ is the heat removed by the coolant. From Equation 1, the parameter of interest Q_{ENV} is obtained by measuring $Q_{COOLANT}$ and $Q_{SUPPLIED}$. As long as the coolant flow rate and inlet temperature remain constant, heat absorbed by the coolant ($Q_{COOLANT}$) from the constant temperature film will remain constant and is independent of the environmental conditions. The actual value of this $Q_{COOLANT}$ is obtained from a measure of the $Q_{SUPPLIED}$ in an environment where $Q_{ENV} \longrightarrow 0$. $Q_{SUPPLIED}$, at any time is obtained by measuring the current in the network required to maintain T_S constant. In effect then, under operating conditions,

$$Q_{ENV} = Q_{SUPPLIED} \text{ (when } Q_{ENV} \longrightarrow 0) - Q_{SUPPLIED} \quad \ldots\ldots \quad 1\,B$$

The Q_{ENV} measured in this way then may be interpreted in terms of the parameters of interest of the flow field by means of an accurate heat transfer relation. The purpose of the present experimental investigation was to obtain this heat transfer relation under conditions of such variables and variable ranges that are likely to be encountered in the application of cooled film sensors to laminar and turbulent flames and hypersonic wakes.

I. 2. Since Q_{ENV} is predominantly due to forced convection, then the forced-convective heat transfer relation for single cylinders in incompressible cross-flow is required. Further, the relation must be valid for the following cases:

a) when the transfer of heat is from the environment to the cylinder,

b) when the temperature difference between the cylinder and the environment is large,

and c) when the environment is composed of flows of different gases and gas mixtures.

I. 3. For forced convective heat transfer between single cylinders and incompressible cross-flows under near-isothermal conditions (or on the basis of the assumption that the fluid properties are independent of temperature), a dimensional analysis of the pertinent parameters gives the following relation:

$$\left(\frac{hd}{k}\right) = f\left(\frac{Vd}{\nu}, \frac{c_p\mu}{k}\right) \qquad \ldots\ldots \quad 2$$

However, for large temperature difference existing between the heat transfer surface and the bulk of the fluid, when a considerable gradient of fluid properties exists in the thermal boundary layer, the above dimensionless groups cannot be uniquely defined. For the purpose of correlation, this so-called temperature loading effect must then be taken into account by evaluating the fluid properties at suitable mean temperatures - arithmatic mean, weighted arithmatic mean, logarithmic mean, geometric mean, or even the individual fluid properties at

different temperatures. Since the temperature loading effect is empirical, the choice depends solely on the success and convenience in the evaluation and application of the correlation.

However, it is to be realized that for non-isothermal cases, a consideration of the dimensionless groups evolved for near-isothermal cases alone does not suffice for the condition of dynamic similarity. The condition of dynamic similarity is that the same ratios must exist between the significant fluid properties at geometrically equivalent points. Since the gradient of properties, being dependent on the temperature ratio, will vary with a variation of temperature loading, a dynamic similarity deficiency may be expected between cases of different temperature loadings. For complete dynamic similarity then, a temperature ratio must be included in the dimensionless relation, so that,

$$\frac{hd}{k} = f\left(\frac{Vd}{\nu}\ ,\ \frac{c_p\mu}{k}\ ,\ \text{temperature ratio}\right) \qquad \ldots\ldots\ 3$$

If it is quite possible that the nature of the similarity deficiency with temperature loading will be different depending on the direction of heat flow, then two relations of the above form are necessary to describe the two processes - heating and cooling. In these relations the fluid properties may now be evaluated at any of the temperatures - T_∞ , T_s or a suitable mean temperature, and the temperature ratio may be obtained by any combination of any two of the temperatures. In line with some of the more successful previous investigations we may choose the arithmatic mean temperature for the evaluation of all the fluid properties (1, 2, 3, 4) and a ratio of T_∞ and T_M for the temperature ratio (1), so that:

$$\frac{hd}{K_M} = f\left(\frac{Vd}{\nu_M}\ ,\ \frac{c_{pM}\,\mu_M}{K_M}\ ,\ \frac{T_\infty}{T_M}\right) \qquad \ldots\ldots\ 4$$

where the subscript M refers to the arithmatic mean temperature.

However, a correlation of the above dimensionless groups still fails to

give a unique expression for the heat transfer process as is apparent by a consideration of the following points.

a) Considering the fact that for a particular fluid the properties of the fluid do not vary with temperature in the same way at different temperature levels, it may be expected that the fashion the group $\left(T_\infty / T_M\right)$ enters in the heat transfer expression, i.e., the temperature loading factor, will be different at different temperature levels. By the same token it will also be dependent on the range of temperature considered. Thus, a correlation may not hold for cases differing from the case for which the correlation was obtained with respect to the temperature loading factor and an evaluation of the correlation at the particular temperature level and range of interest becomes necessary.

b) Apart from a particular fluid at different temperature levels, we may also consider a group of fluids at similar temperature levels. If the variation of the transport properties with temperature of the fluids considered are not identical, then it becomes necessary to evaluate the temperature loading factor individually for each fluid. Since inclusion of the group $\left(T_\infty / T_M\right)$ in the heat transfer expression is to account for the shift in similarity of the fluid property gradients, the 'property ratios' may have to be considered directly in the correlation in place of the temperature ratio, to give a unique relation valid over a group of fluids. Since for a particular gas the significant transport properties vary nearly identically with temperature, variations in all the properties may be lumped together by considering a ratio of values of any one of them. Considering kinematic viscosity as the property, we obtain the more general expression,

$$\frac{hd}{K_M} = f\left(\frac{Vd}{\nu_M}, \frac{\nu_\infty}{\nu_M}, \frac{c_{pM}\,\mu_M}{K_M}\right) \qquad \ldots\ldots 5$$

I. 4. In light of the above discussion and the conditions stipulated in Section 2, we may now formalize the purposes behind the present investigation as follows.

a) To investigate the nature of the temperature loading factor for heating of cylinders in cross-flow for high temperature loadings.

b) To investigate, in terms of improved uniqueness of the correlation, whether it is worthwhile to replace the ratio $\left(T_\infty / T_M\right)$ by $\left(\gamma_\infty / \gamma_M\right)$, when different gases and gas mixtures are considered at high temperature loadings.

c) To investigate whether the slight variation in Prandtl number (due to temperature loading and due to the flow being of different gases and gas mixtures) is significant enough for it to be considered in the heat transfer relation.

d) To obtain a general correlation for forced convective heat transfer for the conditions stipulated in Section 2.

5. The ranges of variables considered in the present investigation were as follows.

a) Reynolds number: The R_{e_M} (based on cylinder diameter) range considered was 5 - 75. However, only data from the range R_{e_M} = 5 to 40 were correlated.

b) Temperature loading: The maximum environment temperature (T_∞) considered was around 1500°K, a limitation imposed by uncertainties in the evaluation of the fluid properties above that temperature. The cylinder temperature (T_s) range considered was 350°K to 550°K. Thus, the temperature loading range achieved was $\frac{T_\infty}{T_s}$ = 2 to 4.

c) Flow composition: The flows were composed of N_2 and He and mixtures of N_2 - He, N_2 - CO_2 and He - CO_2. For each mixture at least two mixture ratios were considered. However, only data from He and N_2 flows were considered for the statistical analysis while the rest of the data were checked against the result of this analysis. The Prandtl number range amongst data for the statistical analysis was Pr = .72 - .75.

II. REVIEW OF PREVIOUS INVESTIGATIONS

II. 1. Considerable data are available for forced convective heat transfer from heated cylinders in air cross-flow (1, 2, 3, 5, 6, 7, 8, 9, 10). On the other hand, data are scarce for the case of heat transfer to cooled cylinders (11, 12, 13). McAdams (14) has collected and correlated results from some of these sources. However, due to misinterpretation of the more important original data, McAdams' correlation must be considered somewhat approximate (for elaboration on this point see Ref. 4). Douglas and Churchill (4), recorrelating some of the data considered by McAdams along with some more recent results, indicated that a unique correlation is possible for cases of heating and cooling over a wide range of temperature loading by evaluating all the fluid properties in the correlation at the arithmatic mean temperature. However, considering the remaining discrepancy in results between different investigations under dissimilar and even similar cases, it is to be concluded that such a general correlation is at best an engineering approximation and may not be suitable for accurate instrument work.

Among the data considered by Douglas and Churchill (4) only those of Hilpert (2) and King (6) fall in the low Reynolds number range of our interest, i.e. $Re_m < 100$. However, their data are for heat transfer from heated cylinders. On the other hand, all data for heating of cylinders, i.e. data of Reiher (12), Vornehm (13), and Churchill and Brier (11), are for Reynolds numbers above 300. Still, the data of Churchill and Brier are of special interest since they are the only ones obtained for any real high temperature difference existing between the cylinder (100°F) and the gas stream (580-1800°F).

II. 2. Consideration of temperature loading effect

Among the investigations reported by Douglas and Churchill (4), only those by Hilpert (2) for convection from cylinders and those by Churchill and

Brier (11) for convection to cylinders consider explicitly the temperature loading effect. However, in the former investigation the effect was obtained over a narrow range of Reynolds number. A consideration of this along with the fact that Hilpert's power law correlation is an approximate representation of the data, led Collis and Williams (1) to obtain a more accurate correlation for hot-wire applications. Further, Collis and Williams obtained their correlation under conditions of low turbulence intensity in the free-stream, the significance of the effect of free-stream turbulence on heat transfer had not been realized in previous investigations. The data due to their carefully conducted experiment were correlated in the following form:

$$Nu_M \left(\frac{T_M}{T_\infty}\right)^{-0.17} = A + B\, Re_M^n \qquad \ldots\ldots 6$$

The values of the constants in the different Re_M ranges are shown in Table 1.

Re_M	A	B	n
.02-44	0.24	0.56	0.45
44-140	0	0.48	0.51

TABLE 1

This may be compared to Hilpert's correlation:

$$Nu_M = C\left[Re_M \left(\frac{T_s}{T_\infty}\right)^{0.25}\right]^m \qquad \ldots\ldots 7$$

Table 2 contains the values of the constants in the different Re_M ranges.

Re_M	C	m
1-4	0.891	0.330
4-40	0.821	0.385
40-4000	0.615	0.466

TABLE 2

The important point to note is that both the investigations showed that for forced convective heat transfer from heated cylinders, an increase in temperature

difference is associated with an increase in $\frac{hd}{k_M}$. For heat transfer in the opposite direction then, i.e. heat transfer to cooled cylinders, the opposite effect is to be expected, i.e. $\frac{hd}{k_M}$ will decrease with an increase in temperature difference. This seems reasonable since an increase in temperature difference has opposite effects on the velocity and the temperature gradients as the heat transfer direction is reversed. Consider the case of heat transfer from cylinders, i.e. $T_s > T_\infty$. In this case, viscosity of the fluid near the wall is greater than the viscosity in the free-stream, causing deceleration of the flow near the wall which results in a steeper velocity profile in the aerodynamic boundary layer as compared to the isothermal case. As the temperature difference is increased, the viscosity difference is increased, the deceleration of the flow near the wall is greater and the boundary layer profile is steeper. Since variation of thermal conductivity with temperature is similar to that of viscosity, a similar effect occurs for the temperature profile. On the other hand, when $T_\infty > T_s$, the viscosity near the wall is less than in the free-stream - consequently the flow near the wall accelerates with a flatter velocity profile. As the temperature difference is increased the flatness of the velocity and temperature profiles will increase. From this reasoning, though no conclusion can be reached as to whether $\frac{hd}{k_M}$ will either increase or decrease with an increase of temperature difference for a particular direction of heat flow, it appears clear, however, that the effect of a variation of the temperature difference will be opposite if the direction of heat flow is reversed.

However, Churchill and Brier's (11) results from their experiment with cooled cylinders at $100^\circ F$ in heated nitrogen flow, where the nitrogen temperature was varied systematically from $580^\circ F$ to $1800^\circ F$, shows the effect on $\frac{hd}{k_M}$

with temperature loading to be in the same direction as obtained by Hilpert (2) and Collis and Williams (1) in their experiments with heated cylinders and wire in ambient air flow. Churchill and Brier's correlation is in the following form:

$$Nu_M = 0.60 \; Pr_M^{0.33} Re_M^{0.5} \left(\frac{T_\infty}{T_s} \right)^{0.12} \qquad \ldots\ldots \; 8$$

for a $\frac{dG}{\mu_M}$ range of 300 to 2300.

It is this anomaly in the direction of the temperature loading effect obtained by Churchill and Brier that focussed attention in the present investigation on the determination of the correct temperature loading factor.

II. 3. Consideration of the Reynolds number dependency of the heat transfer

Earlier investigators, notably King (6), for theoretical reasons, presupposed in their correlation the linear dependency of Nusselt number on $(Re_M)^{0.50}$. Kramer (5), analysing results from later experiments, obtained the same form of correlation as King but with modified constants:

$$Nu = 0.42 \; Pr^{0.2} + 0.57 \; Pr^{0.33} \; Re^{0.5} \qquad \ldots\ldots \; 9$$

The exact range of Re and the reference temperature for property value evaluation were not specified.

On the other hand Hilpert's (2) power law correlation (Eqn. 7) though is somewhat approximate and also ignores the finite heat transfer at zero Re_M, nevertheless indicates that the dependency of Nu_M on Re_M is itself a function of Re_M. He noted discontinuities in the slope of the heat transfer curve at $Re_M = 4$ and $Re_M = 40$.

Later more careful experiments with hot-wires (15) tended to show a systematic deviation of observed Nu_M from the Nu_M obtained from King's equation with increasing Re_M.

Collis and Williams (1) provoked by this deviation from King's law and also by the suspected discontinuity at $Re_M = 40$ conducted their experiment very carefully and obtained a Re_M dependency of Nu_M different from that of King's law and also found a discontinuity at $Re_M = 44$. This discontinuity was confirmed by an aerodynamic investigation of the flow-field around the wire by observing the onset of eddy shedding at $Re_M = 44$.

Now, considering Churchill and Brier's (11) analysis of their data it is to be noted that they presupposed the linear relation of Nu_M to $Re_M^{0.50}$. Further, the correlation was obtained by assuming no heat transfer at zero Re_M, i.e. they presupposed the form of correlation as:

$$Nu_M = A\, Pr_M^{0.33}\, Re_M^{0.5} \left(\frac{T_\infty}{T_s}\right)^n \qquad \ldots\ldots \quad 10$$

and obtained the values of the constants A and n. Apart from the assumption as to the Re_M dependency of Nu_M, this form of correlation may be justifiable at higher Re_M, where the heat transfer at zero Re_M is a small percentage of the total heat transfer, but an extrapolation of the correlation to low Re_M may not be accurate enough. It must be noted that their correlation was obtained for $\frac{dg}{\mu_M}$ beyond 300.

Thus, in the present investigation at low Re_M, the determination of the exact Re_M dependency of Nu_M is considered as part of the analysis.

II. 4. Consideration of Prandtl number effect

Kramer's (5) analysis explicitly considers the effect of Prandtl number variation on heat transfer. Data were obtained for air (Pr = .71),

water (Pr = 7.1), white oil (Pr = 29.6), Transformer Oil I (Pr = 35), and Transformer Oil II (Pr = 525). From this correlation (see Equation 9) it appears that if interest is limited to heat transfer with gases only, the effect of the slight difference in Pr for different species will be very small and may not be detectable in an experiment, due to normal data scatter. By the same token the effect of the small variation of Pr with temperature for a particular specie of gas will also be negligible.

Investigations with different gases have not been carried out, all investigators having used air with the exception of Churchill and Brier (11) who used Nitrogen. As such, it is not possible to determine the uniqueness of any temperature loading factor for different gas species - a point to be investigated in the present analysis.

III. DESCRIPTION OF EQUIPMENT, EXPERIMENTAL SET-UP AND MEASUREMENT PROCEDURE

III. 1. Heat transfer measurements were obtained by traversing internally cooled, electrically heated, constant temperature, cylindrical film sensors across the potential core of a plasma jet. The power input to the plasma jet and the plasma gas flow rate were maintained such that not only would ionization be negligible at the jet exit plane but also that recombination of the dissociated species would be complete in the plenum chamber. Binary mixture flows were obtained by mixing the second gas specie with the primary ionization gas in the plenum chamber. Temperature and velocity measurements were carried out by means of a Pt - Pt 10% Rh thermocouple and a pitot probe respectively, both mounted on the same traverse as the cooled-film sensor. All measurements as functions of the traverse distance along the diameter of the jet were recorded on an X-Y plotter. Knowing the relative position of each instrument with respect to the jet axis, point measurements of pitot pressure, thermocouple output and the film sensor bridge voltage were obtained from the recorded profiles.

III.2. Description of Special Equipment

The sensors, probes, electrical circuitry and the sensor cooling water supply system are manufactured by the Thermo Systems Inc., Minneapolis, Minnesota, as standard equipment. The description of the equipment that follows has been obtained from private communication with Dr. L. Fingerson of the company and from their various bulletins, technical notes and instruction manuals, listed as Ref. 16.

III.2.1. Cooled Film Sensor and Sensor Holder

A photograph of the sensor with explanatory sketches is shown in Fig. 2. The loop type sensor is made of vycor tube, .01524 cm. O.D. and .01016 cm. I.D. A thin film of platinum of thickness 1000 - 2000 Å on one limb of the loop acts as the resistance element and is isolated by heavy gold plating ($1\frac{1}{2}$ - 1 mil thick) on the rest of the loop. The length of the sensing element, in the sensors used, is .103 cm. and its resistance around 5 ohms. The sensing element is coated with a film (5000 Å thick) of silicon monoxide to reduce catalytic effects when the sensor is exposed to flame environment.

The sensor is soldered onto the tip of the sensor holder, which serves as an electrical lead and also as the sensor cooling water connection and contains a built-in filter on the water inlet side. The fittings for the electrical connection to the power supply system and the fittings for the coolant line connection to the water supply system are mounted on a fitting plate, as shown in the photograph in Fig. 3A.

III.2.2 Probe

A photograph and a diagram of the probe with the sensor holder assembly inserted are shown in Fig. 3B and in Fig. 4 respectively. A close-up of the probe tip, showing the sensor in operating position, is shown in Fig. 5. The probe is made up of a series of cascading cooling jackets, the cooling jackets in turn made up of a tightly fitting bundle of stainless steel tubes, to provide uniform and near optimal cooling. The probe is provided with a traversing sleeve and a fitting plate containing the fittings for the jacket cooling water connections. When the sensor holder is in place, its fitting plate is attached to that of the probe by means of screws in slots, allowing for a certain amount

of play, so that the holder can be pulled back and the sensor withdrawn inside the probe when it is not in operation.

III.2.3 Sensor Cooling Water Supply System

The sensor water supply system supplies coolant to the sensor at constant pressure, and hence at a constant mass flow rate. It consists of a stainless steel pressure tank of 1 litre capacity which is filled with distilled water and pressurized through a regulator from a nitrogen bottle. A 25 micron filter is connected to the outlet.

III.2.4 Probe Jacket Water Supply System

Ordinary tap water, filtered through a 25 micron filter, is used for probe cooling. The water pressure is maintained around 80 p.s.i.g.

III.2.5 Bridge and Control Circuit

A simplified functional schematic diagram of the circuit is shown in Fig. 6. The platinum film on the sensor is maintained at constant resistance and hence at a constant temperature by placing it across one arm of a bridge. The desired resistance of the sensor (calculated from the desired operating temperature and the cold resistance of the sensor) is obtained by adjusting the resistance deck R_D. A choice of two bridges is possible, one for low energy dissipation (.005 to approximately 0.5 watts), as encountered in usual hot-wire or hot-film operation and the other for higher energy dissipation (up to 40 watts) for cooled-film operation.

Once a voltage is applied across the bridge and the bridge is balanced, the film will be maintained at the desired temperature. Any change in environmental conditions (changes in temperature, velocity or composition), causing

a variation in the rate of heat transfer to or from the film, will tend to vary the film temperature and hence the film resistance, causing an unbalance between the two sides of the bridge. This unbalance is amplified by the bridge amplifier which signals the power amplifier to increase or decrease the power to the sensor, according to the direction of voltage change in the bridge. This feed-back loop has a frequency response of 500 KH_Z.

The system allows measurement of both bridge voltage and actual electrical power supplied to the film. The latter is obtained by means of a power computer which takes values of the bridge voltage and sensor resistance and uses a squaring circuit, amplifier and a voltage divider. The panel meter may be switched either to read the mean bridge voltage or the mean energy dissipation in watts, when the sensor is exposed to a steady state environment. A photograph of the panel along with that of the sensor water supply system is shown in Fig. 7.

A detailed description of the circuit may be found in Ref. 16A.

III.2.6 Cooled Film Sensor Operating Principle

Referring to Fig. 1 we note that for usual constant temperature, cooled-film application, i.e. $T_\infty > T_s$, a heat balance of the system gives:

$$Q_{SUPPLIED} = Q_{COOLANT} - Q_{ENV}$$

If the cooling water inlet temperature and flow rate (i.e. the coolant pressure) is kept constant, $Q_{COOLANT}$ will remain constant. A measure of $Q_{SUPPLIED}$ then will be a measure of Q_{ENV}, i.e., the heat transferred from the environment to the sensor.

For adequate operation it is then mandatory that $Q_{COOLANT} > Q_{ENV}$ (MAXIMUM). If heat transferred to the coolant is less than that absorbed from the environment,

not only does measurement become impossible but the sensor temperature will increase beyond the set value and the sensor may burn out. A proper $Q_{COOLANT}$ may be set by exposing the sensor to a condition of maximum heat transfer and then by adjusting either the coolant pressure or the sensor temperature or both to obtain a $Q_{COOLANT}$ greater than $Q_{ENV\ (MAX)}$. Since a prior determination of $Q_{ENV\ (MAX)}$ is not always possible (viz., as in the case of application in the hypersonic wakes of projectiles launched in free-flight ranges) a rough estimate of the expected maximum heat transfer may be made and from the calibration chart in Fig. 8, the sensor operating temperature and coolant pressure may be determined. As shown in Fig. 8, at a particular coolant pressure the maximum sensor temperature is limited because of coolant boiling inside the sensor resulting in unstable heat transfer to the coolant. In any case the sensor operating temperature should not exceed 550°K for beyond this temperature the sensor resistance becomes unstable.

The sensor is set to operate at the desired temperature by setting the proper resistance in the resistance deck. The operating resistance is obtained by measuring the sensor "cold" resistance and using the relation:

$$R_s = R_c \left[1 + \alpha \, (T_s - T_c) \right]$$

where R_s is the sensor resistance at the selected operating temperature T_s and R_c is the "cold" resistance at temperature T_c (usually room temperature). The temperature coefficient of resistance α is obtained by a calibration of a representative number of sensors or from the manufacturer's quoted figures. A typical calibration curve for α obtained for three sensors from the batch used in the present investigation is shown in Fig. 9.

The value of $Q_{COOLANT}$ is measured by maintaining the sensor at the operating temperature and coolant pressure and exposed to room environment. Since conservatively calculated heat losses from the sensor due to radiation, free convection and conduction together add up to be two orders of magnitude less than the heat transferred to the coolant, all the heat transferred under room condition may be considered to be transferred to the coolant, i.e.

$$Q_{SUPPLIED\ (at\ room\ temperature)} = Q_{COOLANT}$$

$Q_{COOLANT}$ may be measured directly in electrical units by using the power computer or by measuring the bridge voltage and using the following relation (refer to Fig. 6):

$$Q = \frac{E_t^2 \quad R_s}{(R_s + R_2 + R_{comp})^2}$$

where E_t = bridge voltage

R_s = sensor resistance

R_2 = resistance of the top leg of the bridge

R_{COMP} = probe and cable resistance

For the measurement of $Q_{SUPPLIED}$ under operation the same two methods may be used. However, since there was some doubt as to the calibration of the power computer, in the present investigation it was the bridge voltage that was recorded.

III. 3. Experimental Set-up

A schematic and a photograph of the experimental set-up is shown in Figs. 10 and 11 respectively. The hot jet was obtained by means of a bench

mounted Plasmadyne plasma torch fitted with a nozzle, the nozzle exit diameter being 1/2 in. The gas flow rates were metered by means of calibrated flow meters and pressure gauges mounted on the control panel of the plasma torch. The measuring instruments, i.e., the cooled film sensor probe, the thermocouple and the pitot were mounted on a traversing table. A close-up photograph of the instruments and the plasma torch is shown in Fig. 12. The traverse distance of the table along and across the jet were monitored by a knife-edge slider fixed to the table and sliding over a calibrated linearly variable potentiometer. The cross-traverse potentiometer output was connected to the 'X' input of a Mosley X-Y plotter, whereas the axial traverse potentiometer reading was displayed on a John Fluke differential vacuum tube voltmeter.

A Pt - Pt 10% Rh thermocouple with a bead diameter of .127 cm was used to measure temperature. It was thought to be more judicious to use an unshielded thermocouple and to correct for radiation and conduction loss rather than to use a shielded thermocouple with uncertain radiation effect. Further, the minimum size limitation and the vulnerability of the shielding to high temperature with consequent geometry change precluded the use of shielded thermocouples.

For velocity measurements a carbon-tipped pitot probe with an orifice size of .103 cm was used. The pitot pressure was measured by means of a calibrated MKS Baratron type 77 pressure meter using a type 774 pressure head.

The thermocouple mv output, the pressure meter output and the bridge voltage of the film sensor were connected to the 'Y' input of the X-Y plotter through a control box, so that during a run as each instrument would traverse across the jet their outputs could be successively switched onto the 'Y' input of the recorder for recording. The recording station arrangement is shown in Fig. 13.

The cross traverse distance was recorded at double scale for better positional resolution, whereas the outputs of each instrument were recorded on a scale to give the maximum deflection on the recorder. A typical recording of a run is shown in Fig. 14.

III.4. Measurement Procedure

III.4.1 Instrument Alignment

Before each set of runs (usually consisting of 4 to 5 runs) the sensing elements of the measuring instruments were aligned to be in the same horizontal and vertical planes, the horizontal plane being that of the jet axis and the vertical plane that of the cross-traverse, i.e., normal to that of the jet axis. The cooled film sensor was aligned to be accurately normal to the jet axis. The alignment of the instruments was achieved by a microscope replacing the plasma-jet on its brackets such that the axis of the jet would coincide with that of the microscope as shown in Fig. 15, and by a theodolite placed at a slight angle to the vertical plane of the instruments. Alignment was ensured by traversing each instrument successively to the microscope axis and adjusting its positions such that they coincide with the cross-hairs of both the microscope and the theodolite. After alignment the positions of the instruments with respect to the jet axis and each other were noted by traversing them to the microscope axis and recording the cross-traverse potentiometer output on the X-Y plotter.

During alignment the physical condition of the sensing elements as to deposition of contaminant on the cooled film, flaking of the film, and thermocouple geometry alteration were checked.

III.4.2 Plasma Jet Conditions

Power Setting

The plasma jet was run at very low power inputs so that the temperature at the nozzle exit never exceeded 2000^{o}K. This was to ensure that no part of the gas flow was ionized. Further, the gas flow rates were such that the residence time in the plenum chamber was sufficient for the recombination of the products of dissociation. (The latter condition was verified by the addition of CO_2 in the plenum chamber and noting the absence of any CO flame at the jet exit.)

Jet Stability

The stability of the jet after a 5 minute warm-up period was checked by placing the cooled-film sensor in the jet and recording the bridge voltage on a time scale. Since the film will sense any change in both the velocity and the temperature of the jet, this ensured a check on any drift of both the properties. Over a recorded period of 15 minutes (average time for a run) no drift was noted. However, from time to time the jet would tend to become unstable due to electrode erosion. Readings obtained during these periods were either discarded or retaken.

Jet Turbulence

The turbulence level in the core of the jet was estimated by monitoring the cooled film bridge voltage by an oscilloscope. The maximum cooled-film frequency response is around 10 K.H_Z. Since the film will sense not only the velocity fluctuations but the temperature and concentration fluctuations as well, decoupling of the signal to obtain quantitative measurement of the

intensity of each parameter becomes complicated. From the oscilloscope tracings, a tracing of the superimposed effects of the fluctuation of all the three parameters, in the core of the jet the maximum relative intensity of heat flux was found to be less than 10%. If it is considered that the film is sensing only velocity fluctuations, the most acute situation, then the error in heat transfer measurement will be less than 2%. (See Ref. 17 for an elaboration on the effect of large turbulence fluctuations on heat transfer.) The error due to temperature fluctuation will arise because of consideration of the fluid properties evaluated at the average temperature rather than a consideration of the average of the fluid properties - the difference between them being due to the non-linear variation of fluid properties with temperature. Similarly, the error because of concentration fluctuation will be due to the difference between the evaluated properties at the mean concentration rather than the average of the properties - a difference because of non-linear variation of fluid properties with percentage concentration. However, these effects will be small compared to that due to large velocity fluctuation, i.e. due to the lateral turbulence-velocity component perpendicular to the cylinder.

III.4.3 Run Conditions

During stable operation of the jet, the pitot, the thermocouple and the cooled film sensor were traversed across the jet, the last traversing thrice for three different sensor resistances and hence three different temperature settings. Due to the variation of the sensor "cold" resistance from one sensor to another and sometimes from one run to another it was not always possible to set the same three sensor temperatures for all runs. The distances of the

section of traverse from the jet exit were such that the major portion of the traverse would be through the potential core of the jet. A typical recording of a single run is shown in Fig. 14. To obtain measurements over a range of Re_M and temperature loading the flow rate of the gas and the plasma power input were varied. For each gas specie or specie mixture usually three power settings and for each power setting three flow rates were employed. With a particular power setting and flow rate usually three or four traverses at different distances from the jet exit plane were made. For mixture runs, three different mixtures - N_2-He, N_2-CO_2, He-CO_2 were considered. During these runs, usually the major species in terms of mol fraction was used as the arc-gas, the second specie being mixed with this in the plenum chamber. However, CO_2 was never used as the arc-gas. For each mixture two mixture ratios were considered. Due to the volume-flow rate limitation of the plasma-jet, judicious settings for the mixture ratio were not always possible.

IV. DATA ANALYSIS PROCEDURE, RESULTS AND DISCUSSION.

1. The values of thermocouple emf, pitot pressure and the cooled film bridge voltage at any particular point in the traverse were obtained by taking values equidistant from the jet axis from their respective profiles, the position of the jet-axis with respect to each traverse having been pre-recorded as mentioned in Section III 4.1. Such point values were obtained from only the potential core of the jet.

2. The uncorrected temperature was obtained from the millivolt reading of the thermocouple using the calibration tables of Omega Eng. Inc. This temperature was corrected for the error due to radiation from a heat-balance of the thermocouple bead. (See any standard text for elaboration). From an independent approximate calculation, the conduction error was found to be negligible. For the heat balance the thermocouple bead was considered to be a sphere and the forced convective heat transfer coefficient was obtained from Kramer's (5) correlation for spheres and the emissivity factor for the platinum bead as a function of temperature was obtained from Ref. 18. Since, evaluation of the forced convection coefficient demands a determination of flow velocity and the fluid transport properties at the true temperature and since, the velocity interpretation from the pitot pressure is again dependent on the knowledge of fluid density at the true temperature, an iteration process was used to solve for the true temperature.

The transport property values of the gas species and specie mixtures for the above-mentioned temperature correction process and for the subsequent data analysis were calculated from the expressions collected in Ref. 19. Details of the

expressions used may be found in Appendix I.

From the cooled-film bridge voltage outside the jet and from the bridge voltage when the film was at the point of measurement in the jet, the heat transferred from the environment was obtained according to the method discussed in section III. 2.6. The heat transfer coefficient was then determined from:

$$h = \frac{Q_{ENV}}{a\ (T_\infty - T_s)}$$

3. As a preliminary step to data correlation the dimensionless heat transfer coefficient $\frac{hd}{k_M}$ was plotted as a function of Re_M to determine the general trends and the data scatter. The following points were noted. (Fig. 26 may be consulted for this discussion.)

(i) Because of the narrow range of volume-flow rate possible in the plasma-jet the Re_M range obtained for a paticular specie or specie mixture by a variation of the plasma-gas flow rate was rather limited. However, because of the widely differing kinematic viscosities of the species and specie mixtures considered, the overall Re_M range obtained extended from 5 to 75.

(ii) Nu_M data for Re_M more than 55 were above the trend line of the rest of the points (i.e. those below $Re_M = 40$) when extrapolated to that range. No data were obtained for Re_M between 40 and 55. From previous investigations (1, 2) with heated cylinders a change in slope in the heat transfer curve was noted around $Re_M = 40 - 44$ due to the onset of eddy shedding. However there is no reason to expect the onset of eddy shedding at exactly the same Re_M for the case of cooling of cylinders, since, the boundary layer characteristics in the two cases are different as has been discussed in section II. 2. No aerodynamic investigation specifically aimed at the determination of the onset of eddy shedding was carried

out in the present investigation and hence, any conclusion as to the exact Re_M of discontinuity in the heat transfer curve and as to the reason for the higher Nu_M for Re_M greater than 55 will be deferred until further experimentation. For the present analysis the range of Re_M considered was 5 to 40.

(iii) The scatter of data from the gas mixture runs were noted to be slightly more than those from the pure gas runs. Possibly this is due to imperfect mixing of the gases in the plenum chamber of the jet. For this reason and also because of less certainty in the property value evaluation of mixtures at high temperatures, the subsequent statistical analysis was confined to data from pure He and N_2 flows only.

(iv) Due to the narrow range of Re_M obtained for a particular gas specie or specie mixture and due to the data scatter the expected slight influence of the very small variation of Prandtl number on heat transfer could not be properly detected. In any case, since the statistical analysis was to be confined to date from He and N_2 flows, the Prandtl numbers being very nearly identical for the two gases, consideration of Prandtl number as a variable was not considered important.

4. In the light of the above discussion, it was decided to correlate the data from pure He and N_2 flows, between $Re_M = 5$ and $Re_M = 40$, by a relation of the following form:

$$Nu_M \left(\frac{T_\infty}{T_M}\right)^{n'} = A' + B' \, Re_M{}^{m'}$$

The values of the constants n', A', B' and m' to be determined by a least square fit. The values of the constants were evaluated separately for N_2 and He flows

to determine whether the temperature loading effect is different for the two cases. Further, the values were evaluated individually for the two cases of temperature loading. Once when the loading was applied by a variation of Ts while T_∞ was constant and again when T_∞ was varied while Ts was kept constant. This was done to determine whether a weighted mean temperature rather than the arithmatic mean temperature was more suitable for the evaluation of fluid property. However, since for the individual cases the Re_M ranges were limited, the value of the constant m' was evaluated by considering all data togher, and using this value of m', the values of n', A', B' were calculated for each case. The result of this analysis is shown in the table in Fig. 16 . The n' values were found to be somewhat different for the two cases, though for a particular gas the values were close for the two types of temperature loading.

5. The next step was to replace the temperature ratio by a kinematic viscosity ratio in the analysis, so that the correlation form now became:

$$Nu_M \left(\frac{\nu_\infty}{\nu_M}\right)^n = A + BRe_M^m$$

The values of the constants evaluated for each case and when all He and N_2 data were considered together are shown in the table in Fig. 17. Compared to n' values the values of n were found to be close for the different cases. It remained now to consider whether a unique relation is possible. The fits of the data from each case were checked with the overall relation whose constants were evaluated by considering all He and N_2 data together and as shown in the table in Fig. 17. The worst increase in r.m.s. error was less than 2.5%.

The results of this analysis is shown graphically in Figs. 18 to 26. Figs 18A and 19A are Nu_M vs. Re_M plots of the data from N_2 and He flows respectively for the temperature loading obtained by a variation of T_∞ while T_s was kept constant.

In Figs. 18B and 19B are shown the same data but with the temperature loading factor included. Figs. 20A and 21A and 20B and 21B are similar plots but for data obtained when the temperature loading was applied by keeping T_∞ constant while T_s was varied.

The next step was to consider the temperature loading effect on data from the mixture flows. Considering the lower accuracy in the evaluation of mixture transport properties, it was felt that the significance of the T.L.F. obtained for the mixture flows individually would be ambiguous and in any case not more significant than the value already obtained for He and N_2 flows. As such the data from the mixture runs were checked for the elimination of the temperature loading effect by using the T.L.F. obtained for He and N_2 flows. Figs. 22A, 23A and 24A show Nu_M data from He-N_2, N_2-CO_2 and He-CO_2 mixture flows respectively (two mixture ratios considered for each mixture), plotted as a function of Re_M. Figs. 22B, 23B and 24B are replots of the corresponding data but considering the T.L.F. A considerable improvement in data scatter may be noted, though no claim to the complete elimination of the temperature loading effect can be made.

All data corrected for the temperature loading effect plotted together are shown in Fig. 25. It is evident that except for CO_2-N_2 data which were for Re_M greater than 55, data below $Re_M = 40$ overlap and follow the same heat transfer curve and as such show that along with a unique T.L.F. a unique correlation is also possible. Finally, the obtained Re_M dependancy of the Nu_M

was checked for the different specie mixture flows by plotting the data on $Nu_M\left(\frac{\nu_\infty}{\nu_M}\right)^{.15}$ vs. $Re_M^{.45}$ grid, as shown in Fig. 26. The r.m.s. deviation of Nu_M from the correlation line was found to be .0924 when all data below $Re_M = 40$ were considered together.

6. Comparing the correlation obtained in the present investigation, i.e. :

$$Nu_M = (0.2068 + .4966\ Re_M^{0.45})\ \left(\frac{\nu_\infty}{\nu_M}\right)^{-.15}$$

with previous correlations (see section II), the following points may be noted.

(i) It is found that for the case of heat transfer to cooled cylinders, as the temperature loading is increased, the hd/k_M is decreased. This is consistent with the previously observed (1,2) increase in hd/k_M with increasing temperature loading for the case of heat transfer from heated cylinders, as has been elaborated in section II, 2. However, from Churchill and Brier's (11) result for similar direction of heat flow as in the present investigation the opposite effect is noted.

(ii) In the Re_M range of 5 to 40, the Nu_M was found to vary linearly with $Re_M^{.45}$. This deviation from King's law is similar to that observed by Collis and Williams (1) in their experiment with heated wires. However, there is no reason to expect the same law to hold for both the cases of cooling and heating, since as previously discussed, the aerodynamic features in the two cases are different. A valid comparison exists only with correlations obtained for similar direction of heat flow. However, Churchill and Brier's analysis presupposed a linear Nu_M variation with $Re_M^{.5}$ and as such can not be properly compared to the present result.

(iii) Finally Fig. 27 compares values of Nu_M calculated from some of the correlations obtained for heat transfer from heated cylinders with values calculated from the present correlation, the evaluation being for an identical condition of

heating of cylinder with $T_s = 400^{\circ}K$, $T_\infty = 1200^{\circ}K$ and the flow composed of N_2. Even considering the wide discrepancies in values calculated from correlations obtained for cooling of cylinders only, the error involved in using them to predict heat transfer for heating of cylinders is quite apparent.

V. CONCLUSIONS

1. For forced convective heat transfer to circular cylinders placed normal to a heated flow, a correlation was obtained statistically from data measured in the Reynolds number range of 5 to 40, temperature loading range of $\frac{T_\infty}{T_s}$ = 2 to 4 and for flows of N_2 and He. Over the entire range the following correlation was determined,

$$Nu_M \left(\frac{\nu_\infty}{\nu_M}\right)^{.15} = .2068 + .4966\ Re_M^{.45}$$

where all the fluid properties in the dimensionless parameters are evaluated at the arithmatic mean temperature.

2. Because of increased data scatter and also because of some uncertainty in the property value evaluation of mixtures at elevated temperatures, data from the binary mixture flows composed of any two gases from the gas species He, N_2 and CO_2 were not included in the statistical analysis. However, these data were checked for fitness with the correlation. The r.m.s deviation of Nu_M from the correlation line was found to be .0924 when all data below Re_M = 40 were considered together.

3. Due to the narrow range of Re_M investigated for a particular specie or specie mixture and also due to the data scatter, the expected slight influence of the small variation of Prandtl number (because of the consideration of different species and specie mixtures and also because of variation of temperature), could not be discerned.

4. Replacement of the usual temperature ratio in the temperature loading factor by a viscosity ratio enabled a unique correlation to be derived for flows composed of gas species whose transport property value variations with temperature

are different.

5. The direction of the temperature loading effect, i.e., in the present investigation for heating of cylinders a decrease in hd/k_M with an increase in temperature loading, is consistent with previously observed increase in hd/k_M with an increase in temperature loading for the case of cooling of cylinders.

6. The Re_M dependency of Nu_M was found to be different from that according to King's law as also observed in previous investigations with hot wires. However, due to absence of previous data for the case of heating of cylinders, no direct comparison could be made.

7. A discontinuity in the heat transfer curve was noted between $Re_M = 40$ and $Re_M = 55$. Unfortunately, no data were collected between these values of Re_M, and since no specific aerodynamic investigation was carried out to determine a change in the flow features in this range, no firm conclusion as to the exact Re_M and nature of the discontinuity can at present be made.

8. Finally, a comparison of the Nu_M values calculated for the case of heating of cylinders from correlations obtained specifically for cooling of cylinders with Nu_M obtained in the present experiment (for heating of cylinders), clearly shows the need for two separate correlations for the two directions of heat transfer. The error involved in predicting heat transfer in the opposite direction may not be negligible, specially when significant temperature loading is involved.

ACKNOWLEDGEMENTS

This work was performed under contract to CARDE and was supported partly by D.R.B. Grant 9550-06 to Professor S. Mölder, Director, Hypersonic Propulsion Laboratory of McGill University.

Thanks are due to the following staff members and personnel of McGill University : Professor S. Mölder for his overall supervision; Messrs. L. Vroomen and J. Kelly for assistance with the instruments, Professor J.M. Forde for reading the manuscript, and Mr. R. Quinton for his assistance in the details of publication.

Thanks are due also to the following members of CARDE staff : Mr. G.H. Tidy for his cooperation, Mr. I.R. Cameron for permission to use the plasma-jet facility, and Messrs. D. Ellington, F. Christie, G. Trottier, G. Guerin, P. Desjardins and M. Verreault for their general assistance.

REFERENCES

1.	Collis, D.C.; Williams, M.J.	Journal of Fluid Mechanics, 6, 357 (1959)
2.	Hilpert, R.	Forsch. Gebiete Ingenieurw., 4, 215 (1933)
3.	Van der Hegge Zijnen, B.G.	Appl. Sci. Research A, 6, 129 (1956)
4.	Douglas, W.J.M., Churchill, S.W.	Chem. Eng. Progr. Symposium, No. 18, 52, 23 (1956)
5.	Kramer, H.	Physica, 12 no. 2-3, 61 (1946)
6.	King, L.V.	Trans. Royal Soc. (London), A214, 373 (1914)
7.	Benke, R.	Arch. Wärmewirtsch., 19, 287 (1938)
8.	Hughes, J.A.	London Phil. Mag., 31, 118 (1916)
9.	Griffiths, E.; Awberry, J.W.	Proc. Inst. Mech. Engrs. (London), 125, 319 (1933)
10.	Small, J.	London Phil. Mag., 19, 251 (1935)
11.	Churchill, S.W.; Brier, J.C.	Chem. Eng. Progr. Symp., No. 17, 51 , 57 (1955)
12.	Reiher, H.	Forsch. Gebiete Ingenieurw., No. 269, 1 (1925)
13.	Vornehem, L.	Reported by J. Ulsamer, ibid, 3,94 (1932)
14.	McAdams, W.H.	"Heat Transmission", 3ed., McGraw-Hill, New York (1954)
15.	Newman, B.G.	Australian Council for Aeronautics, Report ACA-53
16.	Thermo-Systems Inc., Minneapolis, Minnesota	a) Instruction manual b) Tech. Bulletin Nos. 2, 3, 4 c) Brochures d) Private communication
17.	Hinze, J.O.	"Turbulence", McGraw-Hill, New York (1959)

18. Caldwell, F.R. "Temperature - its Measurement and Control in Science and Industry" - Ed. Herzfeld, C.M., Vol. 3, Part 2, Page 81, Reinhold, New York (1962)

19. Brokaw, R.S. NACA T.R.R-81

APPENDIX I

EXPRESSIONS FOR THE CALCULATION OF TRANSPORT PROPERTIES FOR PURE GASES AND GAS MIXTURES

NOMENCLATURE

		UNITS
C_p/R	Dimensionless heat capacity	
K	Thermal conductivity	$\frac{CaL}{cm.\ sec\ {}^{o}K}$
K'	Monatomic thermal conductivity	"
K"	Internal thermal conductivity	"
k	Boltzman constant	erg/^{o}K
M	Molecular weight	g/g -mole
R	Universal gas constant	CaL/mole^{o}K
T	Absolute temperature	^{o}K
x	Mole fraction	
ϵ	Maximum energy of attraction	erg.
μ	Absolute viscosity	g/cm.sec.
σ	Zero energy collision diameter	A
Ω	Reduced collision integral	

SUBSCRIPTS

i, j	Components i and j of a mixture
mix	Entire mixture
n	Number of components in the mixture
1, 2.	Component 1 and 2 of a mixture

APPENDIX I

The following expressions were used to calculate transport property values for non-polar gases and gas mixtures.

i) Viscosity (Refs. 1, 2, 3.)

$$\mu = 26.693 \times 10^{-6} \frac{\sqrt{MT}}{\sigma^2 \Omega}$$

or

$$\mu = 26.693 \times 10^{-6} \left[\frac{1}{\sigma^2}\sqrt{\frac{M\epsilon}{k}}\right]\left[\frac{\sqrt{kT/\epsilon}}{\Omega}\right]$$

ii) Thermal conductivity (Refs. 1, 3.)

$$K = K' + K''$$

$$K' = 198.91 \times 10^{-6} \frac{\sqrt{T/M}}{\sigma^2 \Omega}$$

$$K'' = K' \times 0.88 \left(\frac{2}{5}\frac{C_p}{R} - 1\right)$$

iii) Viscosity of gas mixtures (Refs. 3, 4.)

$$\mu_{mix} = \sum_{i=1}^{n} \frac{\mu_i}{1 + \sum_{\substack{J=1 \\ J \neq i}}^{n} \phi_{iJ} \frac{x_J}{x_i}}$$

where

$$\phi_{iJ} = \frac{\left[1 + \left(\frac{\mu_i}{\mu_J}\right)^{1/2}\left(\frac{M_J}{M_i}\right)^{1/4}\right]^2}{2\sqrt{2}\left(1 + \frac{M_i}{M_J}\right)^{1/2}}$$

iv) Thermal conductivity of gas mixtures (Refs. 3, 4, 5.)

$$K_{mix} = K'_{mix} + K''_{mix}$$

$$K'_{mix} = \sum_{i=1}^{n} \frac{K'_i}{1 + \sum_{\substack{J=1 \\ J \neq i}} \Psi_{iJ} \frac{x_J}{x_i}}$$

where

$$\Psi_{iJ} = \phi_{iJ}\left[1 + 2.41 \frac{(M_i - M_J)(M_i - 0.142\, M_J)}{(M_i + M_J)^2}\right]$$

$$K''_{mix} = \sum_{i=1}^{n} \frac{K''_i}{1 + \sum_{\substack{J=1 \\ J \neq i}}^{n} \phi_{iJ} \frac{x_J}{x_i}}$$

where

$$\phi_{iJ} = \frac{\left[1 + \left(\frac{K'_i}{K'_J}\right)^{1/2} \left(\frac{M_i}{M_J}\right)^{1/4}\right]^2}{2\sqrt{2}\left(1 + \frac{M_i}{M_J}\right)^{1/2}}$$

The dimensionless heat capacity i.e. $\frac{C_p}{R}$ values as function of temperature were obtained from Ref. 6. The reduced collison integral (for viscosity and thermal conductivity) values as function of reduced temperature

$\frac{KT}{e}$ were obtained from Table 1B of Ref. 7. Values for the rest of the constants were taken from Table I of Ref. 3.

REFERENCES FOR APPENDIX I

1. Hirschfelder, J.O.; Curtiss, C.F.; Bird, R.B. — "Molecular Theory of Gases and Liquids", John Wiley (1954)

2. Bromley, L.A.; Wilke, C.R. — Viscosity Behaviour of Gases. Ind. and Eng. Chem. 43, no. 7, 1641 (July 1951)

3. Brokaw, R.S. — Alignment Charts for Transport Properties NACA TR R-81

4. Brokaw, R.S. — Approximate Formulas for the Viscosity and Thermal Conductivity of Gas Mixtures. J.Chem. Phys. 29, no. 2, 391 (August 1958)

5. Hirschfelder, J.O. — Proc. of the Joint Conf. on Thermodynamics and Transport Properties of Fluids. The Inst. of Mech. Eng. (London), p. 133 (1958)

6. Hilsenrath, J. et al. — Tables of Thermal Properties of Gases. Cir 564, NBS (1955)

7. Bird, R.B.; Stewart, W.E ; Lightfoot, E.N. — "Transport Phenomena", John Wiley, New York (1963)

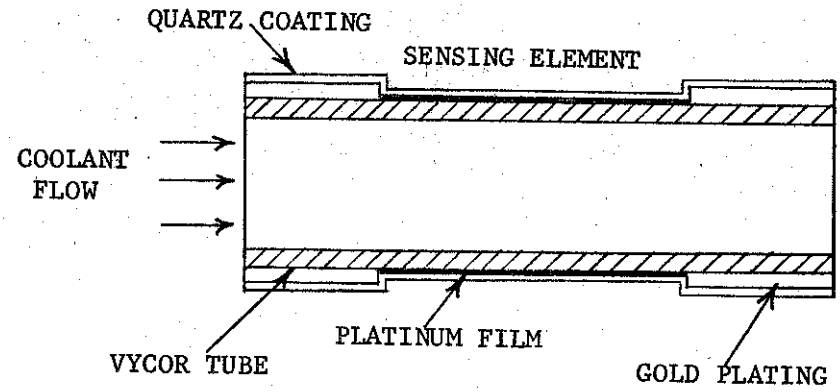

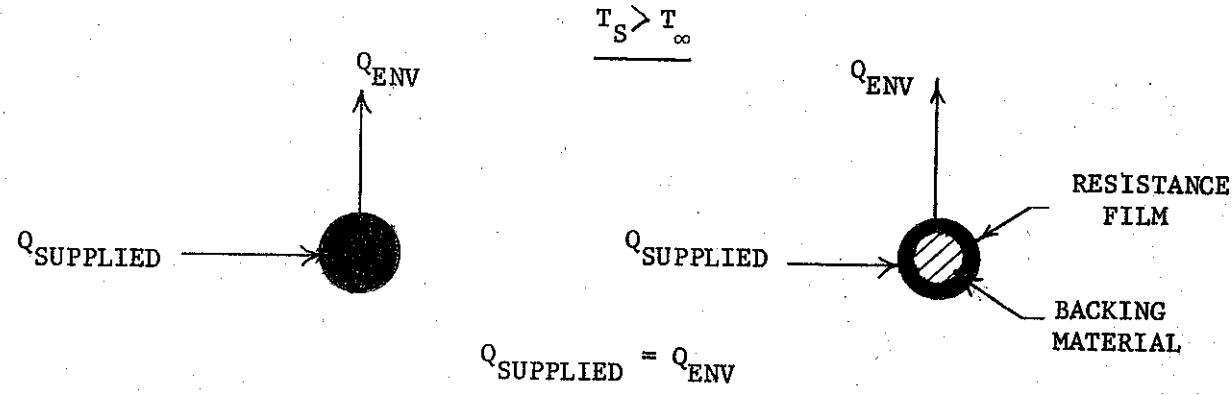

HOT WIRE OR HOT FILM OPERATION

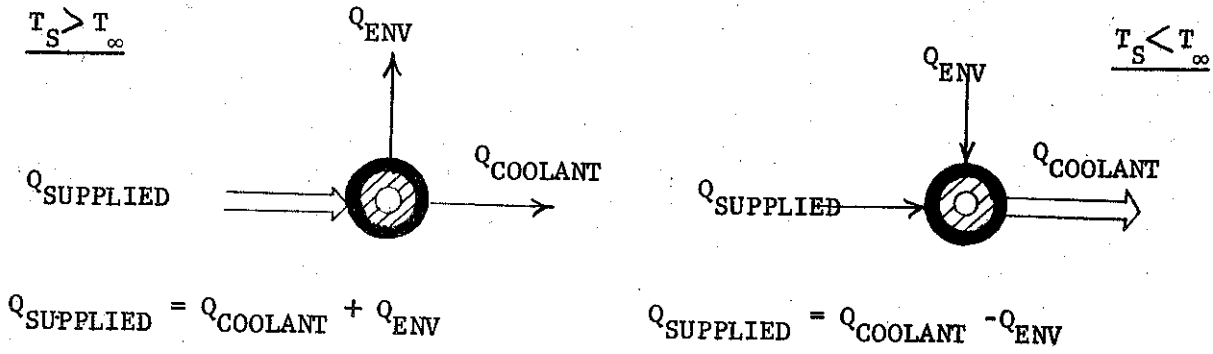

COOLED FILM OPERATION

FIGURE 1 - HEAT BALANCE OF HOT ~~WATER~~ WIRE OR HOT FILM AND COOLED FILM OPERATION

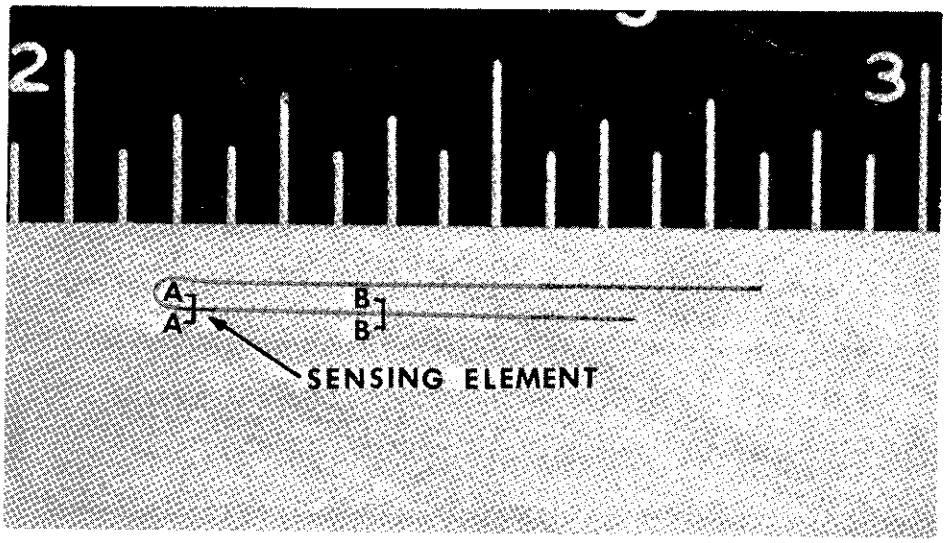

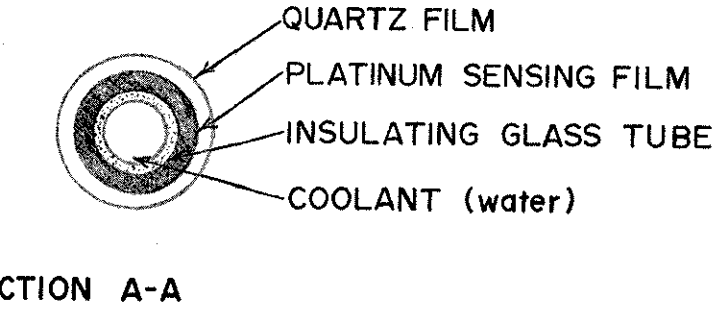

CTION A-A

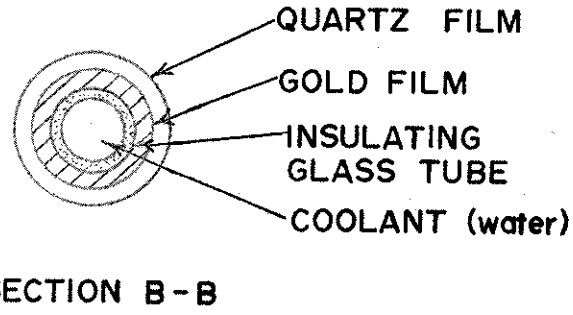

SECTION B-B

FIGURE 2 - COOLED FILM SENSOR (PHOTOGRAPH - MAGNIFICATION x 5, SKETCHES - NOT TO SCALE)

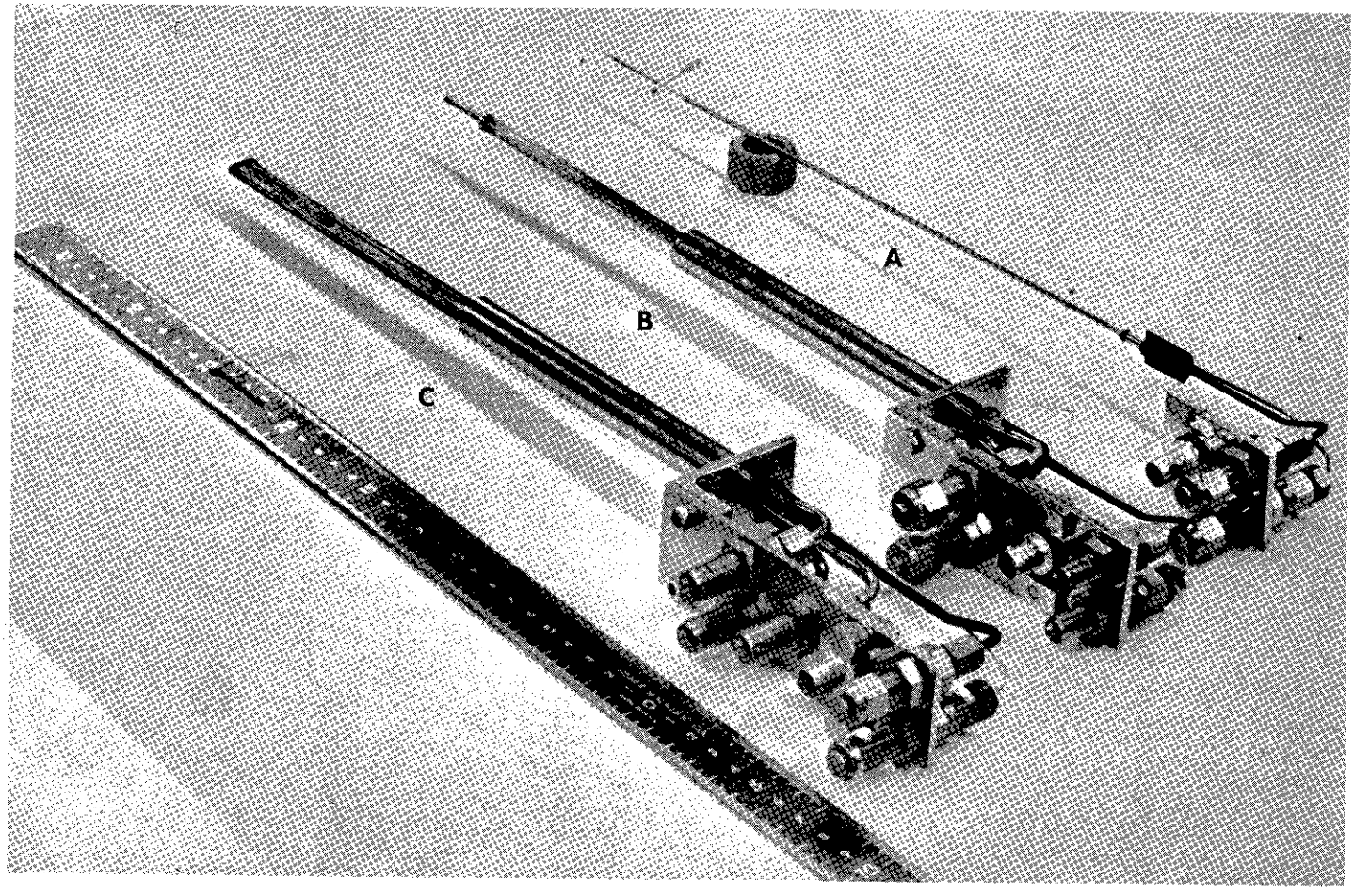

FIGURE 3 - A) SENSOR HOLDER
B) HEAT FLUX PROBE
C) ASPIRATING PROBE

(SCALE IN CENTIMETRES)

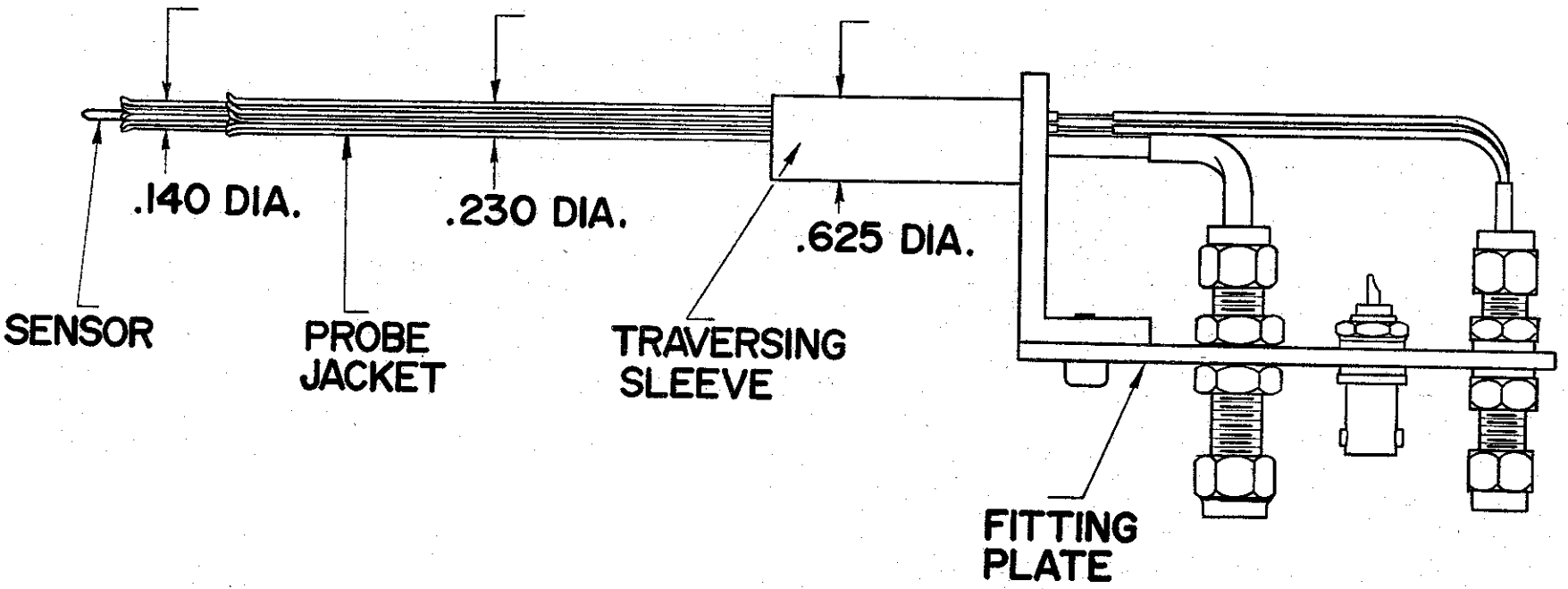

FIGURE 4 - DIAGRAM OF PROBE WITH SENSOR HOLDER INSERTED

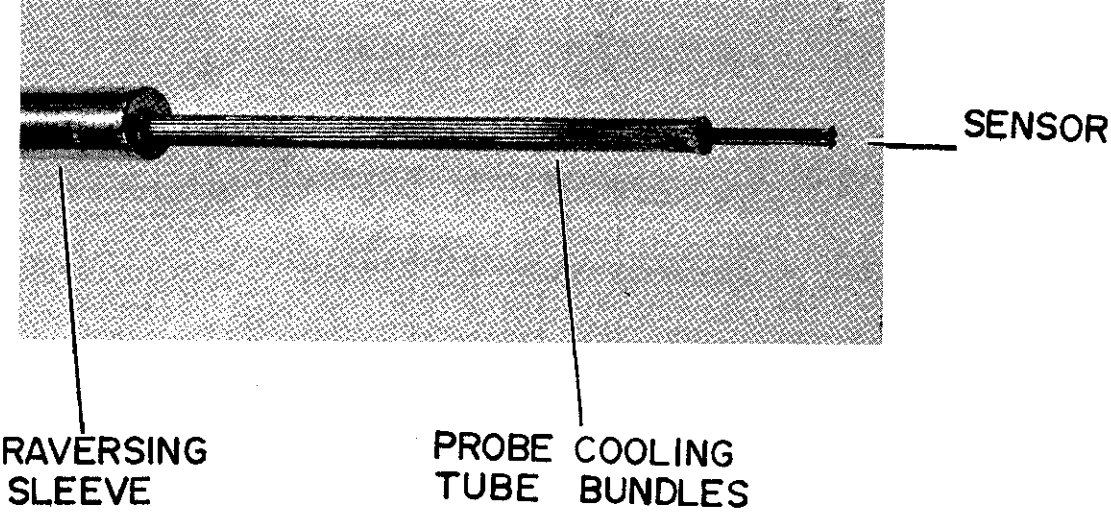

FIGURE 5 - PROBE TIP WITH SENSOR IN OPERATING POSITION

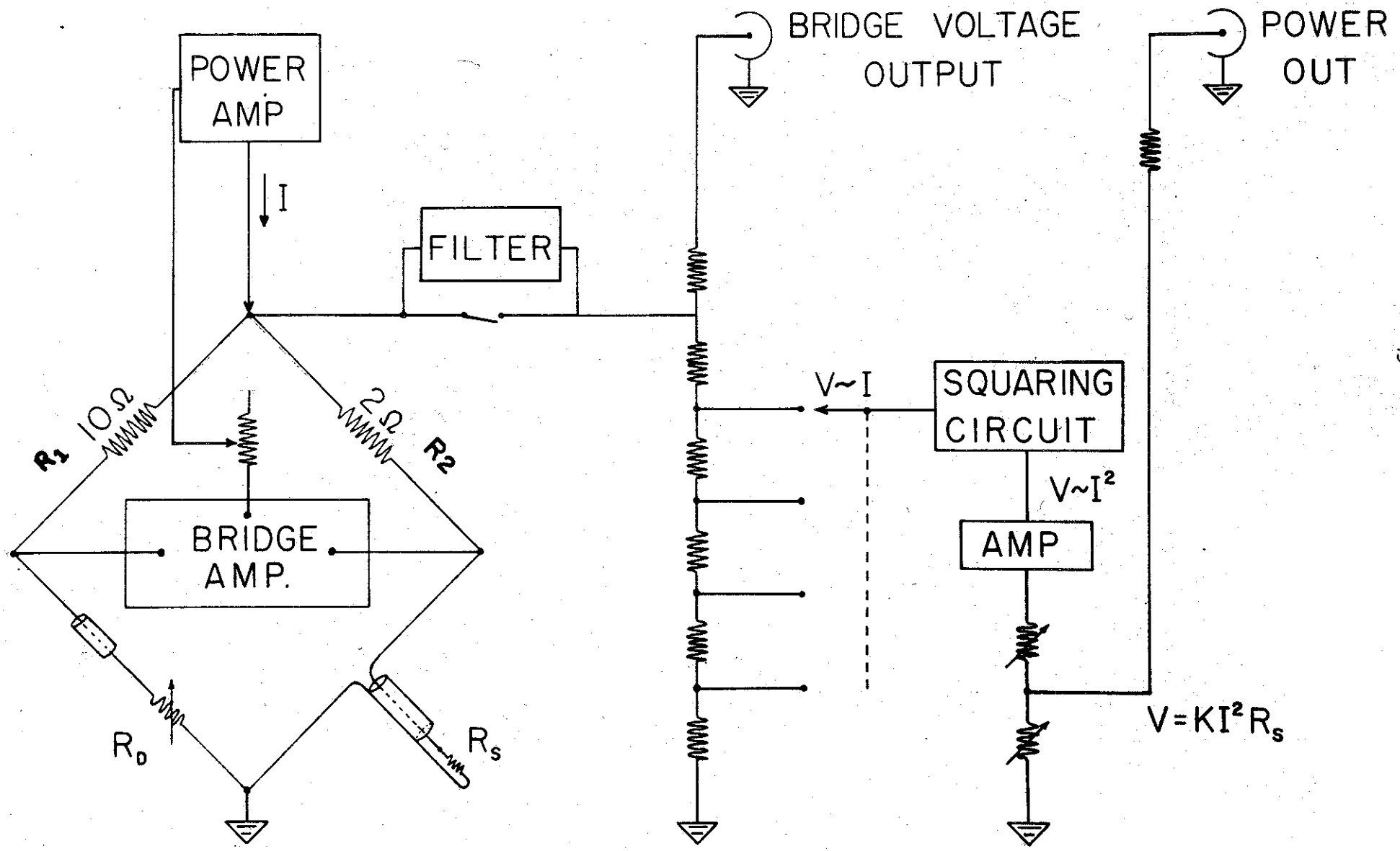

FIGURE 6 - FUNCTIONAL SCHEMATIC OF CIRCUIT

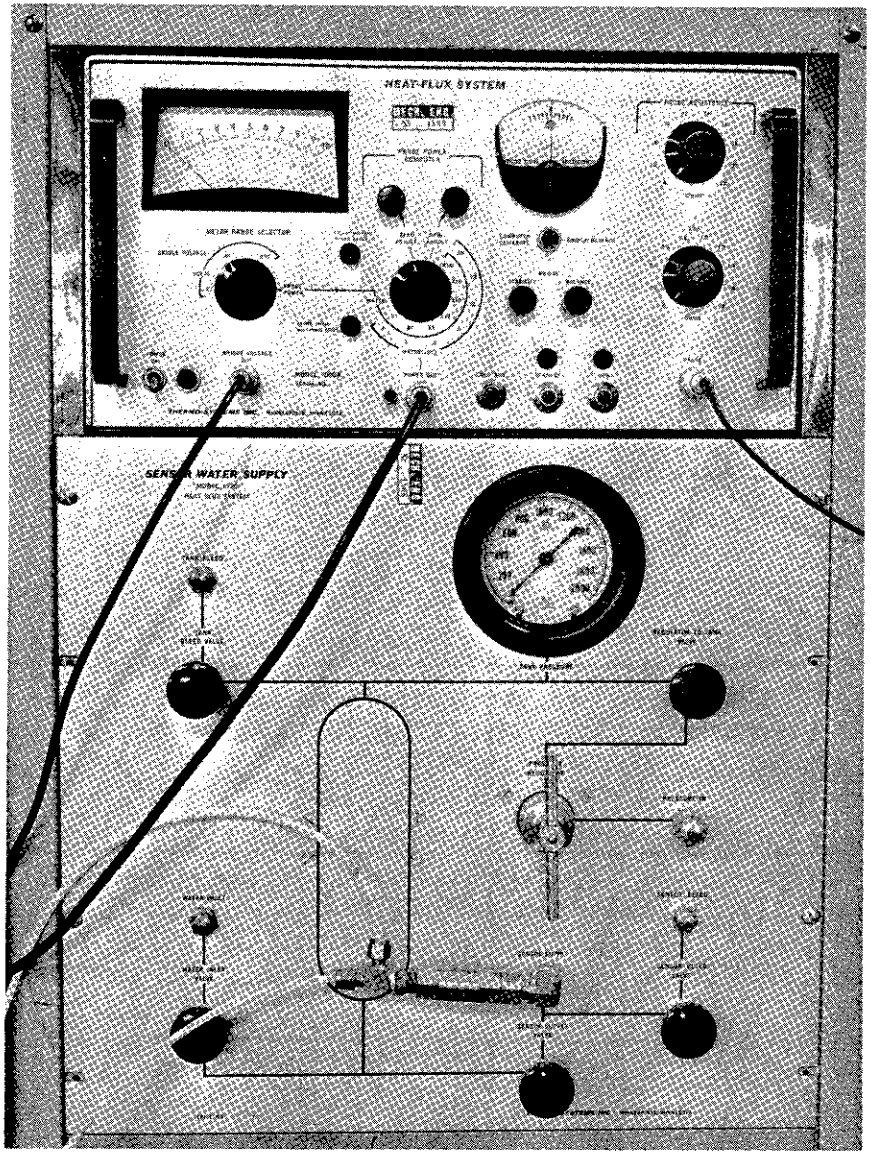

FIGURE 7 - COOLED-FILM CIRCUIT AND SENSOR WATER SUPPLY CONTROL PANELS

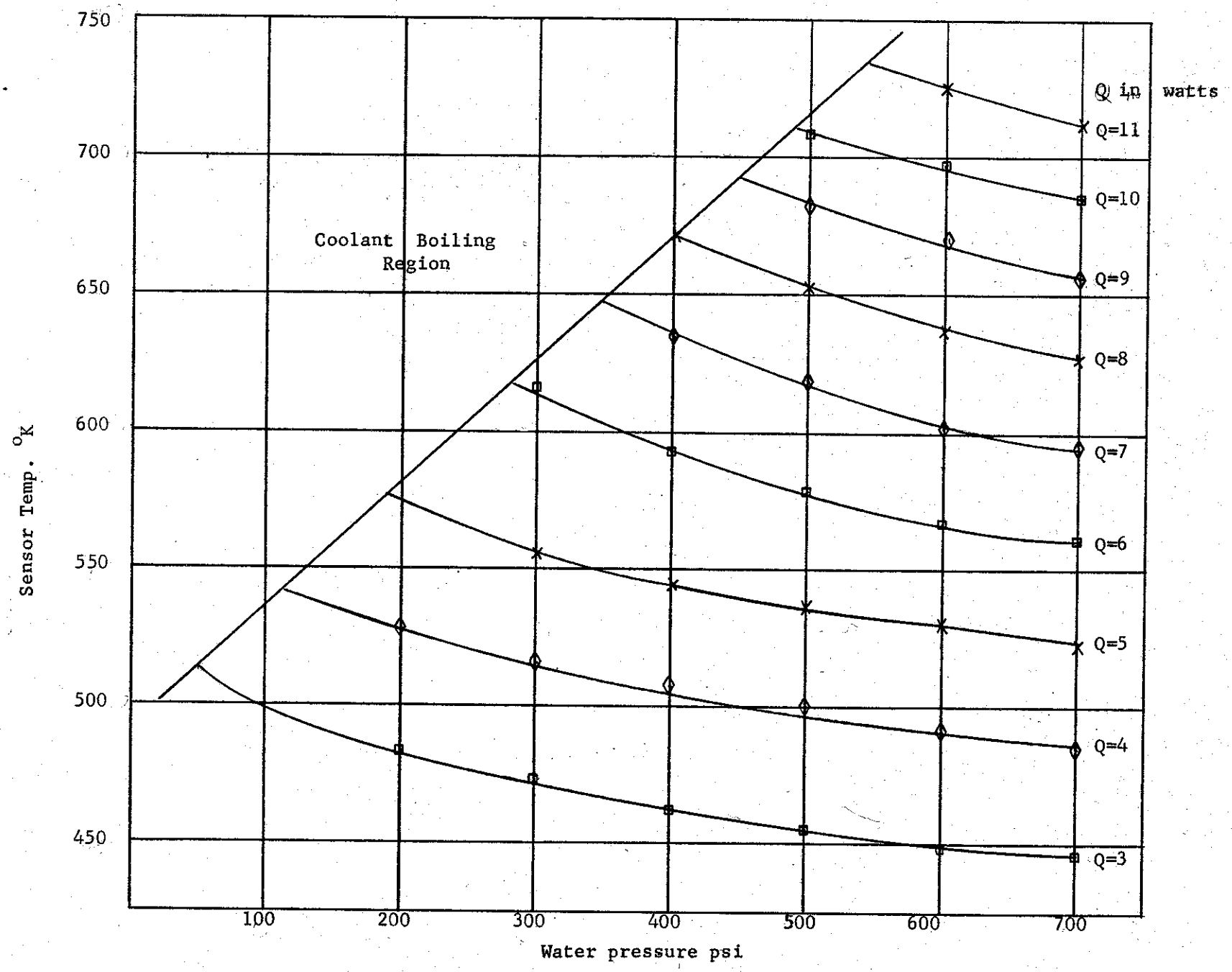

FIG. 8 - CALIBRATION CURVES FOR SENSOR OPERATING TEMPERATURE AND COOLANT WATER PRESSURE

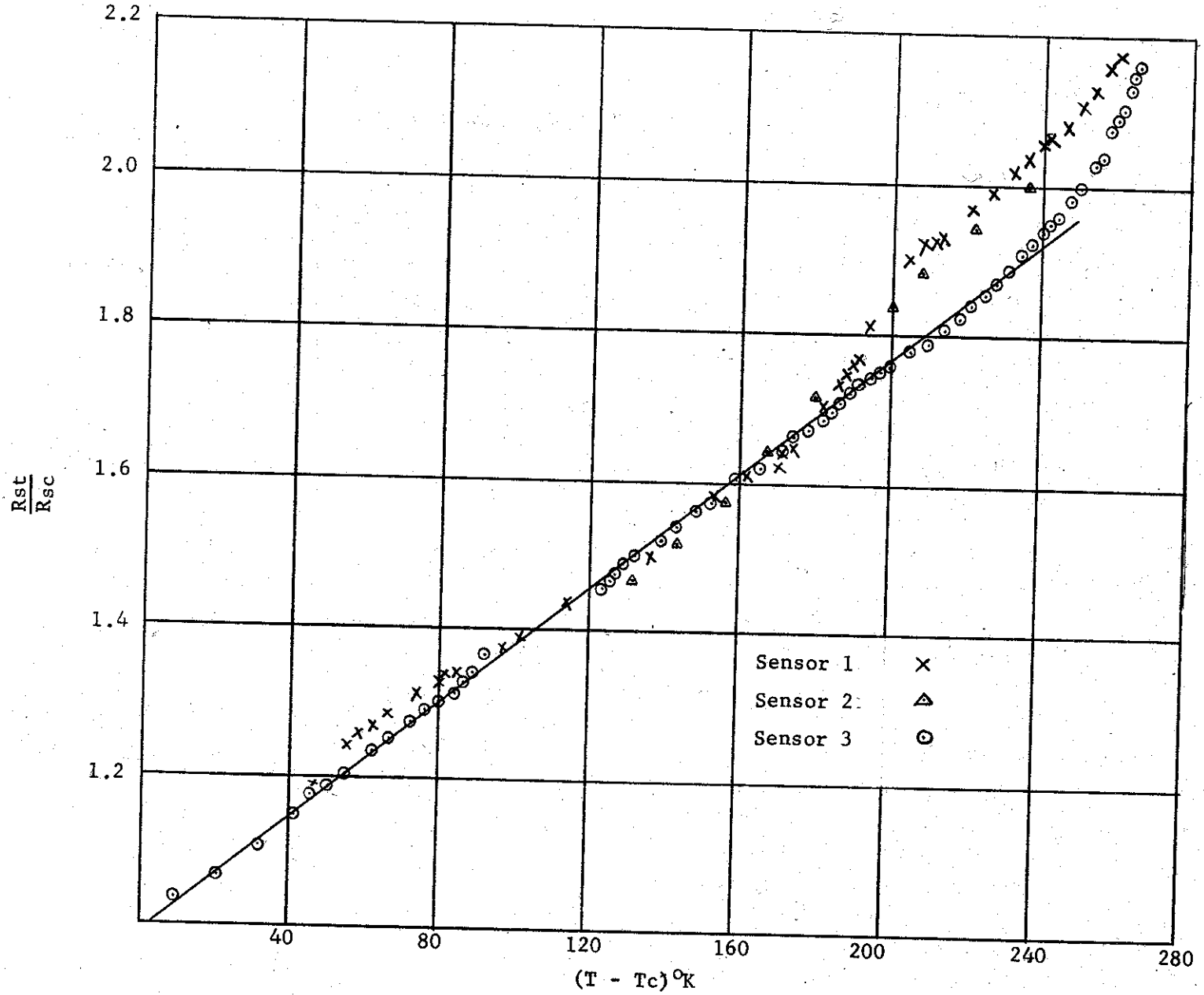

FIG. 9 - A TYPICAL CALIBRATION CURVE FOR α, THE TEMPERATURE COEFFICIENT OF RESISTANCE.

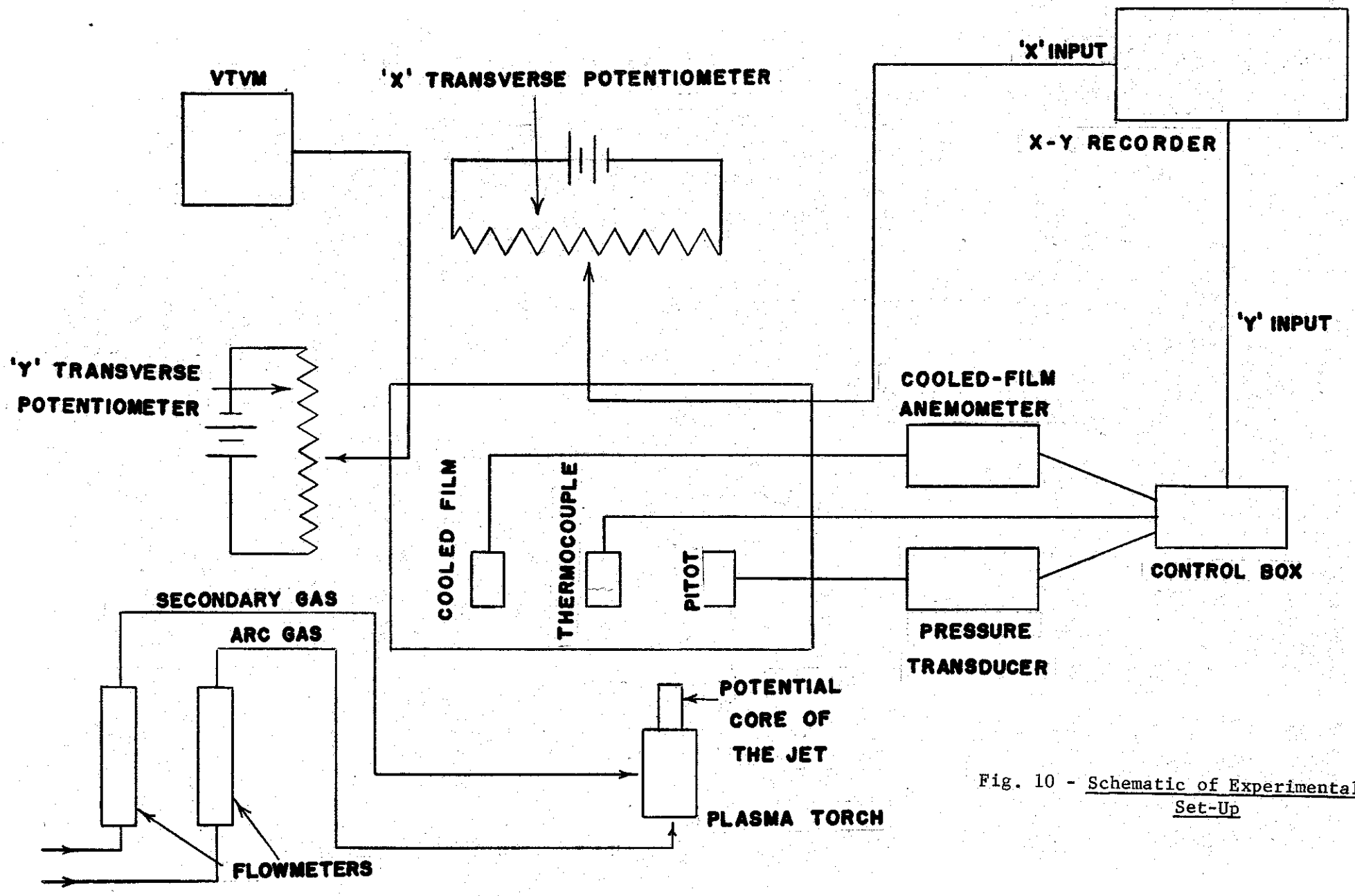

Fig. 10 - Schematic of Experimental Set-Up

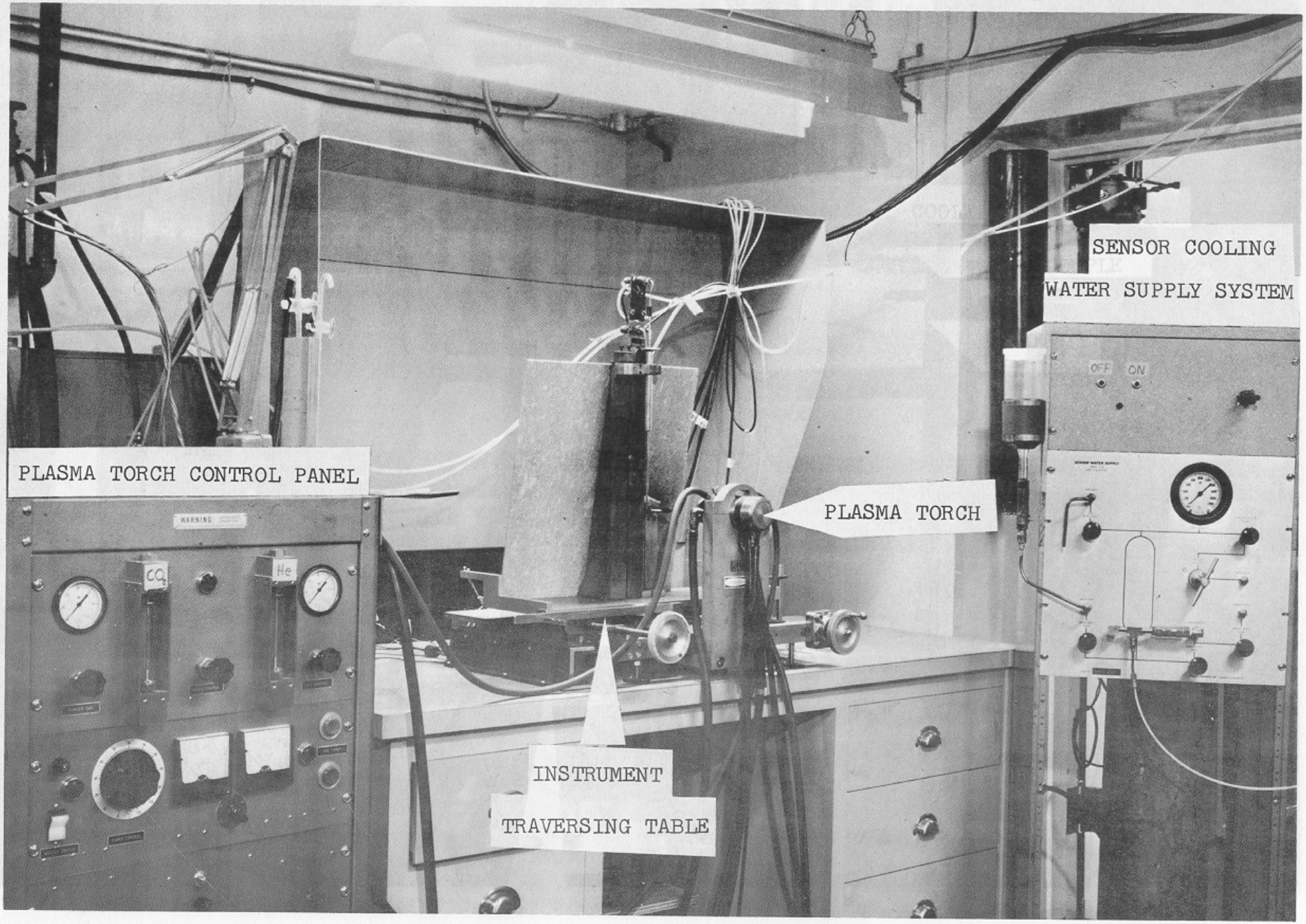

FIG. 11 - GENERAL EXPERIMENTAL SET UP

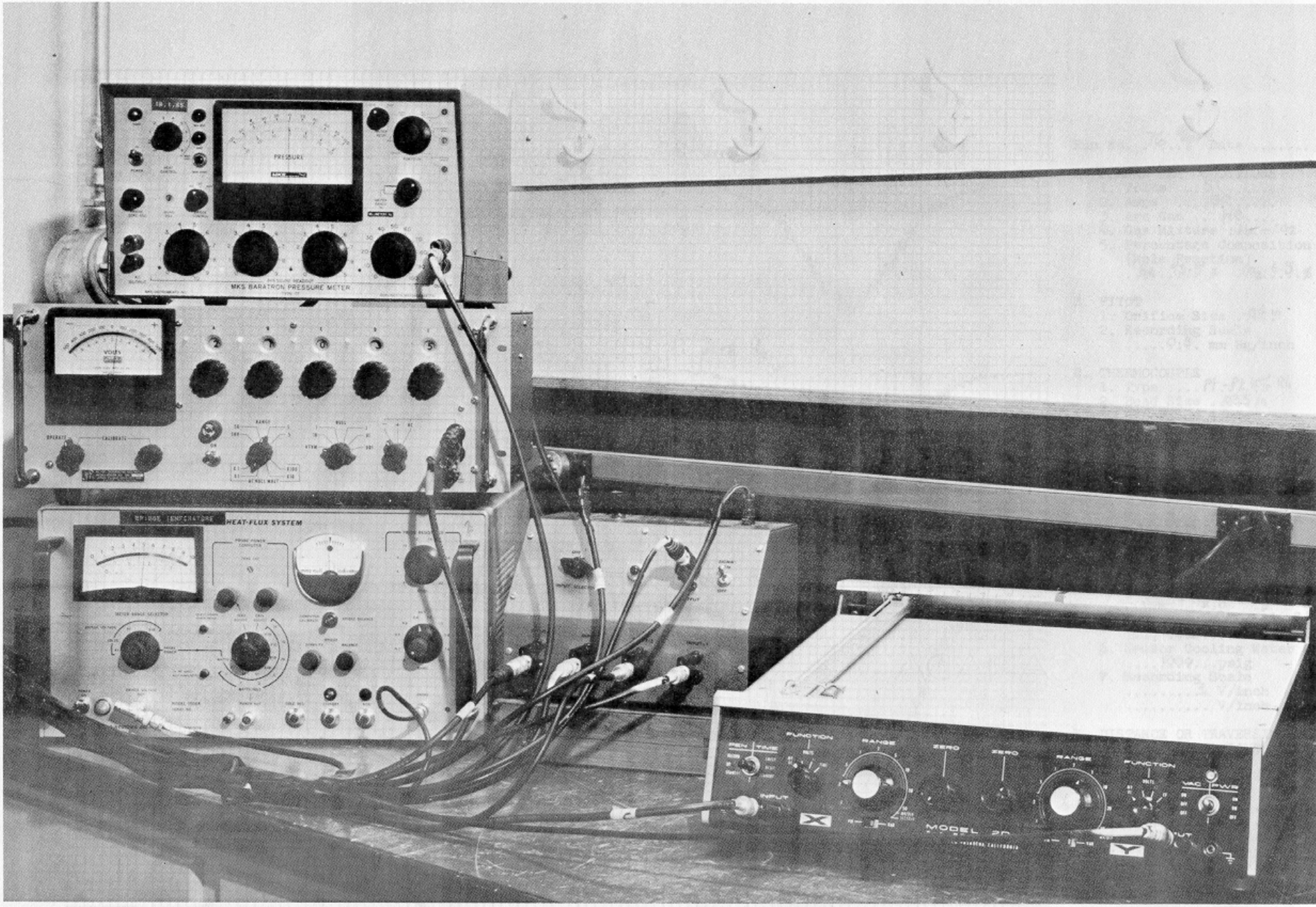

FIG. 13 - GENERAL ARRANGEMENT OF RECORDING STATION

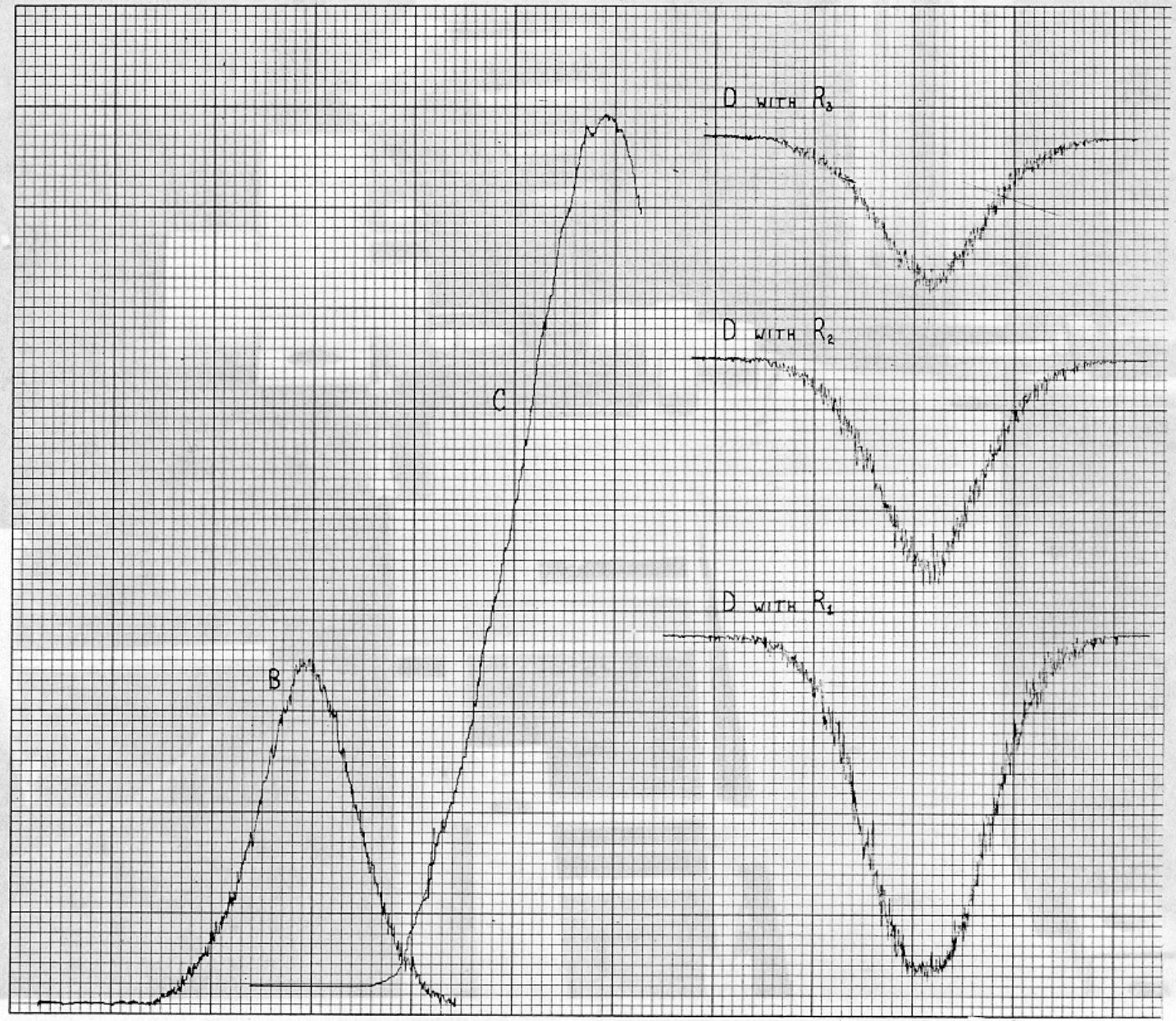

Run No. 76... Date .....

A. PLASMA JET CONDITIONS
1. Volts ...51.....
2. Amps ...150.....
3. Arc Gas ...He....
4. Gas Mixture . He - CO_2
5. Percentage Composition (Mole Fraction)
..He..93.5 % ..CO_2: 6.5 %

B. PITOT
1. Orifice Size .04 in
2. Recording Scale
.....0.9. mm Hg/inch

C. THERMOCOUPLE
1. Type ....Pt - Pt 10% Rh
2. Bead Size .035 in
3. Recording scale
.....1. mv/inch

D. Heat Flux Sensor No. 9....
1. Dia ...:006 in.....
2. Length .:0.6 in...
3. Cold Resistance
$R_c = R_{s,c} + R_p + R_c$ =
.....9.8..... Ω
4. Cable and Probe Resistance
$R_p + R_c$ = .3.03..Ω.
5. Sensor Operating Resistance
$R_{DECK} = R_{s,o} + R_p + R_c$
i) ..10.5..Ω. ii) .11.5...Ω.
iii) 12.5..Ω. iv) .....Ω.
6. Sensor Cooling Water Pressure
....1999...psig
7. Recording Scale
.....1. V/inch
..... V/inch

E. DISTANCE OR TRAVERSING PLANE FROM JET EXIT PLANE .1.7...inch

F. X-SCALE MAGNIFICATION - x 2

G. REMARKS .....
.....
.....
.....
.....

FIG. 14 - A TYPICAL DATA RECORDING SHEET

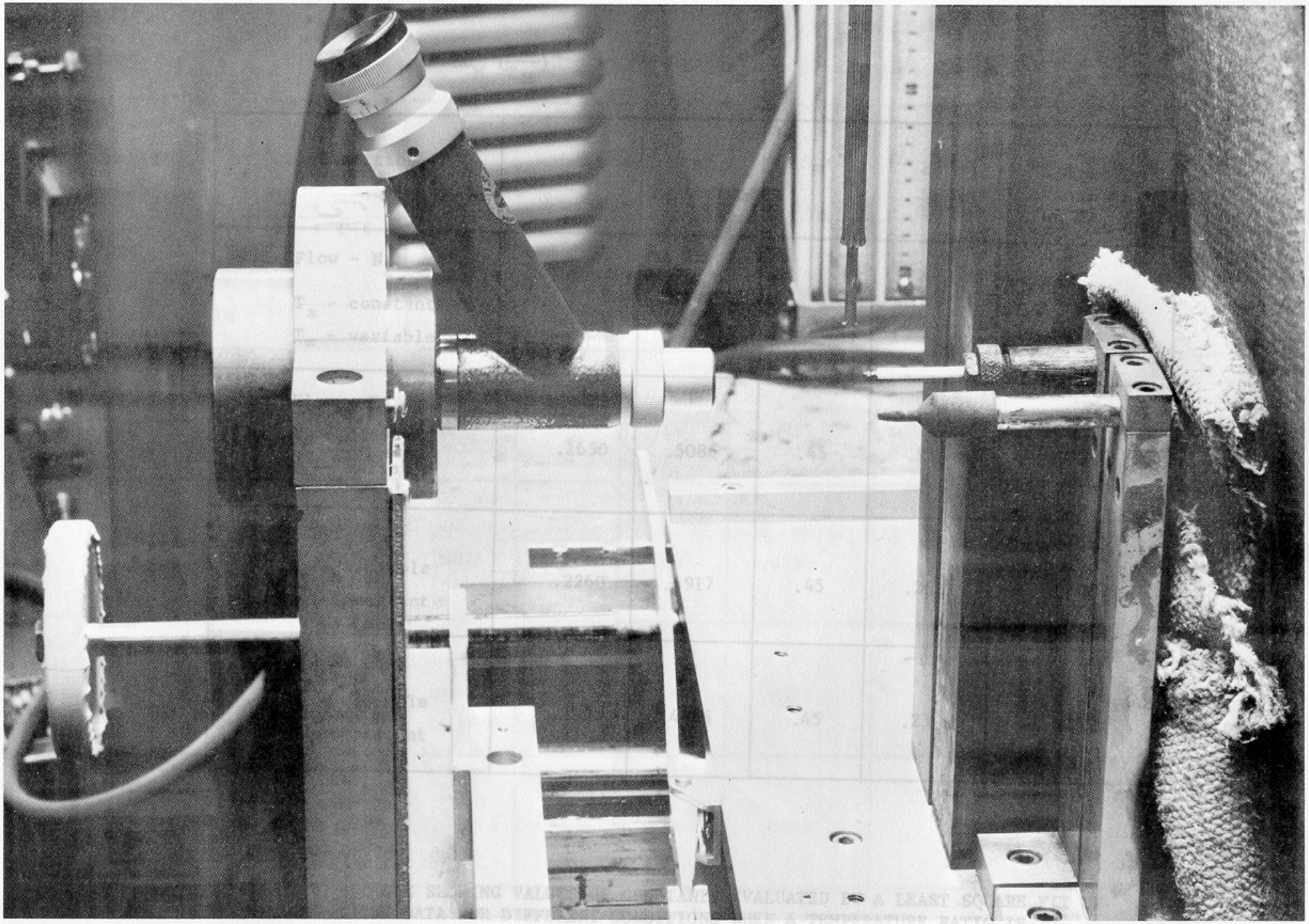

FIGURE 15 - MICROSCOPE IN PLACE OF PLASMA TORCH FOR INSTRUMENT ALIGNMENT

$$Nu_M \left(\frac{T_\infty}{T_M}\right)^{n'} = A' + B' \, Re_M^{m'}$$

Condition	A'	B'	m'	n'	R.m.s. deviation of Nu_M
1. Flow - N_2 T_s - constant T_∞ - variable	.1880	.5092	.45	.26	.0601
2. Flow - He T_s - constant T_∞ - variable	.1690	.5086	.45	.21	.0225
3. Flow - N_2 T_s - variable T_∞ - constant	.2260	.4917	.45	.25	.06002
4. Flow - He T_s - variable T_∞ - constant	.2003	.4936	.45	.23	.02525

FIG. 16 - TABLE SHOWING VALUES OF CONSTANTS EVALUATED BY A LEAST SQUARE FIT OF THE DATA FOR DIFFERENT CONDITIONS WHEN A TEMPERATURE RATIO IS CONSIDERED IN THE CORRELATION.

$$Nu_M \left(\frac{\nu_\infty}{\nu_M}\right)^n = A + BRe_M^m$$

Condition	A	B	m	n	r.m.s. deviation of Nu_M	r.m.s.* deviation of Nu_M	Increase in deviation
1. Flow - N_2 T_s - constant T_∞ - variable	.1890	.5055	.45	.16	.0598	.06009	0.485%
2. Flow - He T_s - constant T_∞ - variable	.1708	.5094	.45	.14	.0224	.0229	2.232%
3. Flow - N_2 T_s - variable T_∞ - constant	.2260	.4925	.45	.15	.0599	.0600	0.167%
4. Flow - He T_s - variable T_∞ - constant	.2011	.4925	.45	.14	.0255	.0261	2.353%
5. Flow - N_2 and He T_s, T_∞ - variable	.2068	.4966	.45	.15	.0385	-	-

* When using constants evaluated considering all He and N_2 data together, i.e. the values in row 5.

FIG. 17 - TABLE SHOWING VALUES OF CONSTANTS EVALUATED BY A LEAST SQUARE FIT OF THE DATA FOR DIFFERENT CONDITIONS WHEN A KINEMATIC VISCOSITY RATIO IS CONSIDERED IN THE CORRELATION

FIGURE 18A - Nu_M Vs Re_M FOR A CIRCULAR CYLINDER IN NITROGEN CROSS-FLOW FOR VARIOUS TEMPERATURE LOADINGS. TEMPERATURE LOADING EFFECT OBTAINED BY VARYING THE FLOW TEMPERATURE AND KEEPING THE CYLINDER TEMP. CONSTANT.

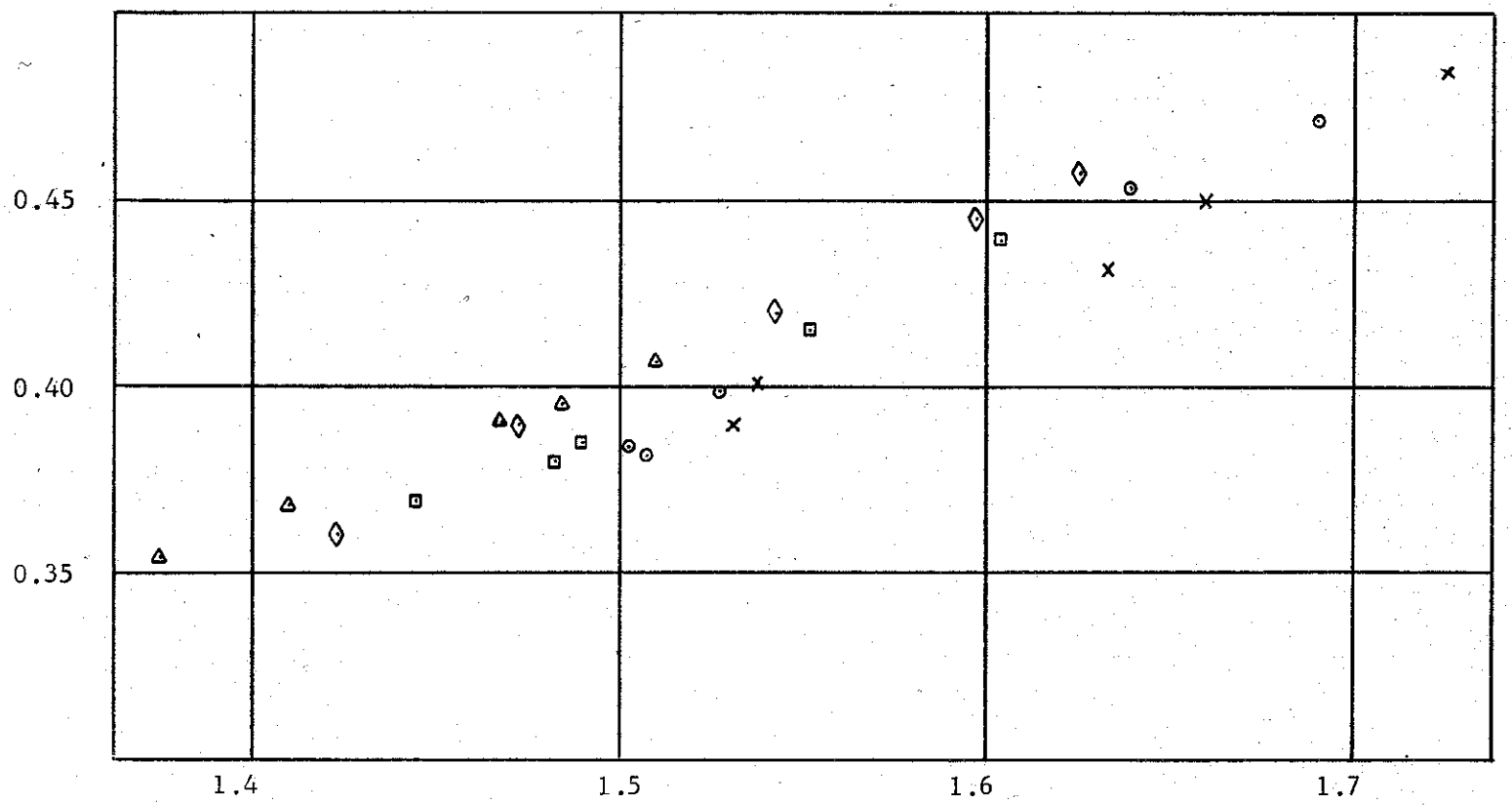

CYLINDER DIA. - .0152 c m.
FLOW - NITROGEN

T_∞ °K	T_s °K	$\frac{T_\infty}{T_M}$	$\frac{\nu_\infty}{\nu_M}$	SYMBOL
1627 - 1660	428	1.583 - 1.590	2.175 - 2.193	×
1435 - 1465	428	1.540 - 1.548	2.073 - 2.090	⊙
1244 - 1263	428	1.488 - 1.494	1.947 - 1.970	⊡
1050 - 1061	428	1.421 - 1.425	1.790 - 1.810	◇
852.4 - 858	428	1.331 - 1.334	1.600 - 1.607	△

FIGURE 18B - $Nu_M (\nu_\infty / \nu_M)^{.15}$ V_s Re_M FOR NITROGEN CROSS-FLOW SHOWING ELIMINATION OF RESIDUAL TEMPERATURE LOADING EFFECT.

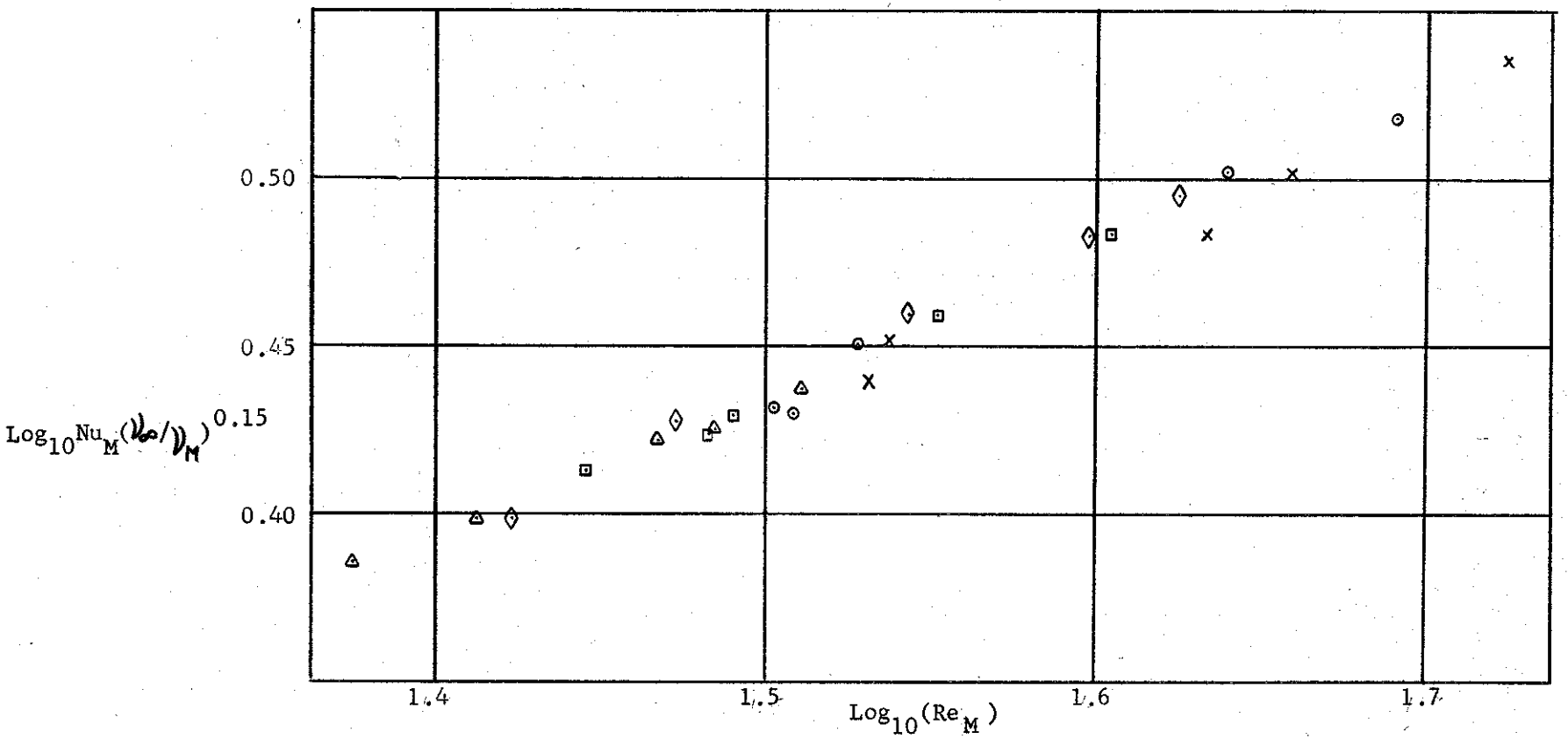

CYLINDER DIA. - .0152 c m.
FLOW - NITROGEN

T_∞ °K	T_s °K	$\frac{T_\infty}{T_M}$	$\frac{\nu_\infty}{\nu_M}$	SYMBOL	T_∞ °K	T_s °K	$\frac{T_\infty}{T_M}$	$\frac{\nu_\infty}{\nu_M}$	SYMBOL
1627 - 1660	428	1.583 - 1.590	2.175 - 2.193	X	1050 - 1061	428	1.421 - 1.425	1.790 - 1.970	◇
1435 - 1465	428	1.540 - 1.548	2.073 - 2.090	⊙	852.4 - 858	428	1.331 - 1.334	1.600 - 1.607	△
1244 - 1263	428	1.488 - 1.494	1.947 - 1.970	⊡					

FIGURE 19A - Nu_M Vs Re_M FOR A CIRCULAR CYLINDER IN HELIUM CROSS-FLOW FOR VARIOUS TEMPERATURE LOADINGS. TEMPERATURE LEADING EFFECT OBTAINED BY VARYING T_∞ AND KEEPING T_S CONSTANT.

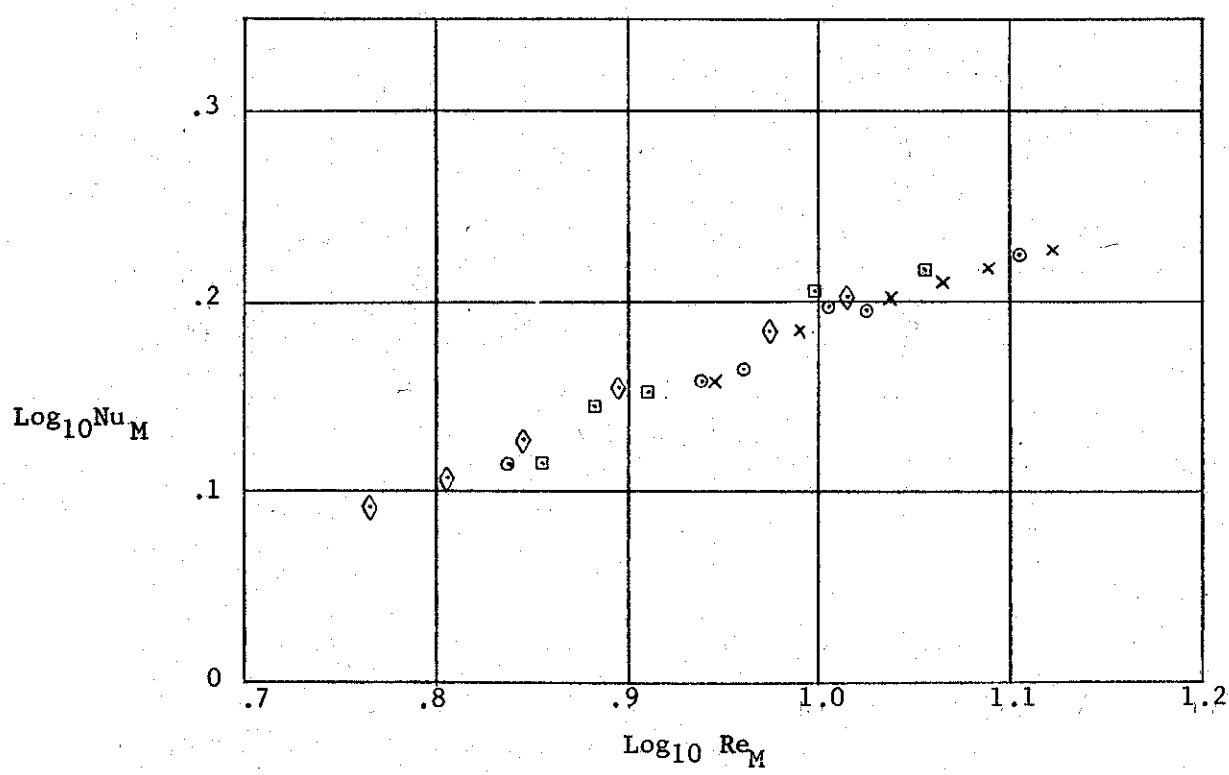

CYLINDER DIA. - .0152 c m.
FLOW - HELIUM

T_∞ °K	T_s °K	$\frac{T_\infty}{T_M}$	$\frac{\nu_\infty}{\nu_M}$	SYMBOL
1356 - 1360	460	1.493 - 1.494	1.910 - 1.920	×
1176 - 1183	460	1.438 - 1.440	1.800 - 1.820	⊙
994 - 997	460	1.367 - 1.369	1.670 - 1.678	⊡
802.7 - 803	460	1.271	1.500	◇

FIGURE 19B - $Nu_M (\nu_\infty / \nu_M)^{15} V_s Re_M$ FOR HELIUM CROSS-FLOW SHOWING ELIMINATION OF RESIDUAL TEMPERATURE LOADING EFFECT

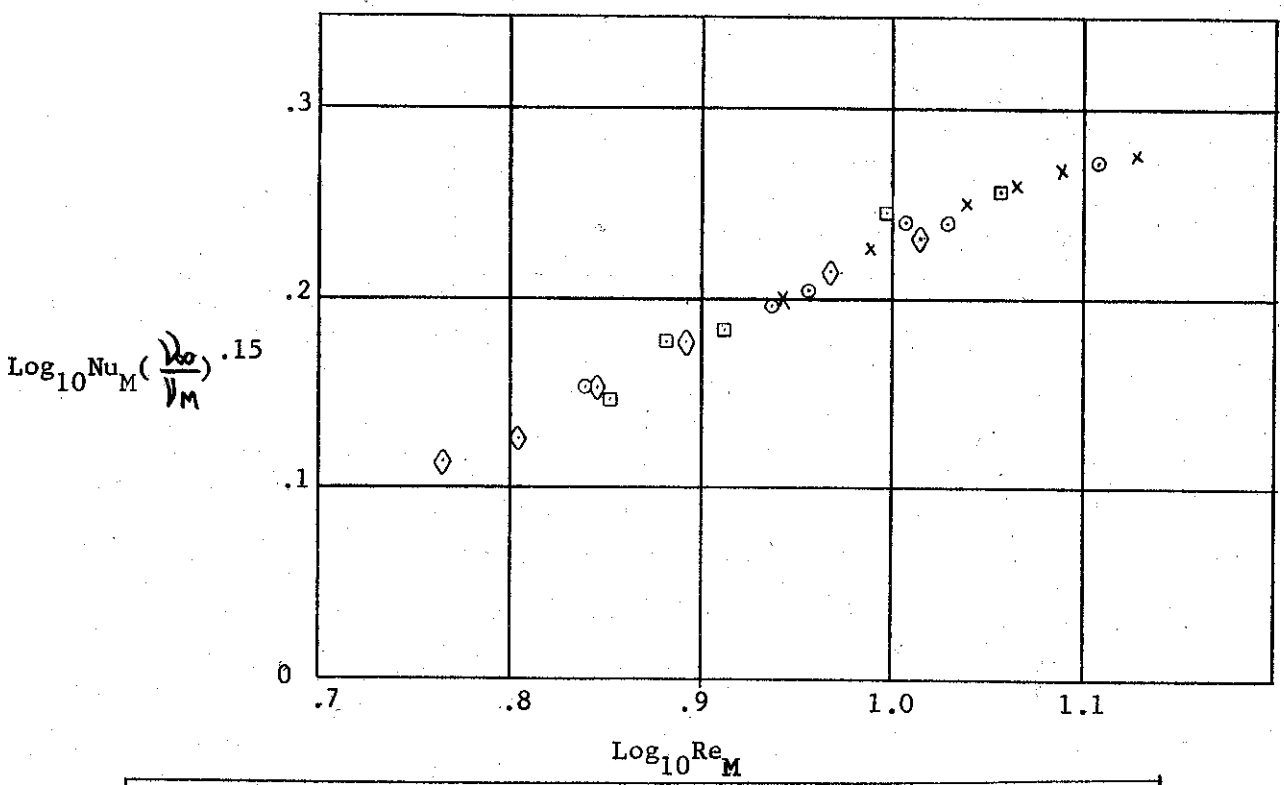

T_∞ °K	T_s °K	$\frac{T_\infty}{T_M}$	$\frac{\nu_\infty}{\nu_M}$	Symbol
1356 - 1360	460	1.493 - 1.494	1.910 - 1.920	×
1176 - 1183	460	1.438 - 1.440	1.800 - 1.820	⊙
994 - 997	460	1.367 - 1.369	1.670 - 1.678	⊡
802.7 - 803	460	1.271	1.500	◇

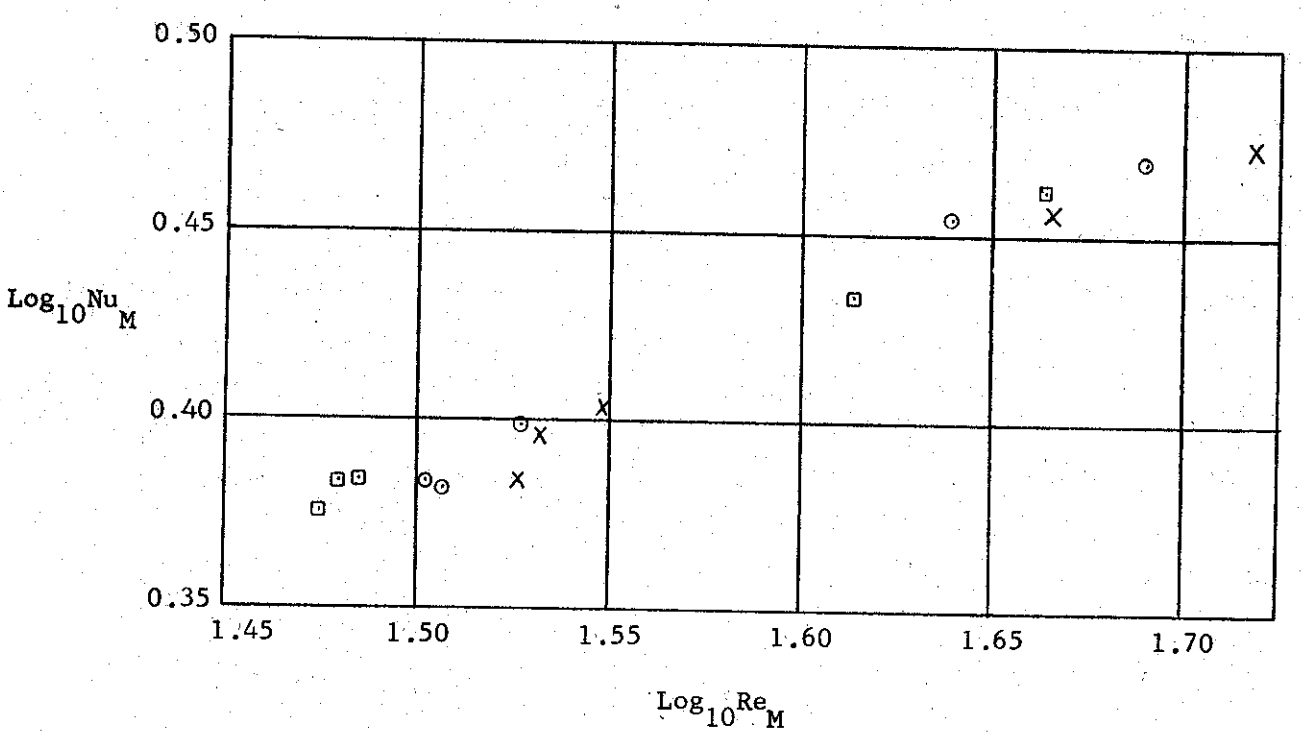

FIGURE 20A - Nu_M Vs Re_M FOR A CIRCULAR CYLINDER IN NITROGEN CROSS-FLOW FOR VARIOUS TEMPERATURE LOADINGS. TEMPERATURE LOADING EFFECT OBTAINED BY VARYING THE CYLINDER TEMPERATURE WHILE KEEPING THE FLOW TEMPERATURE CONSTANT.

CYLINDER DIA. - .0152 c m.
FLOW - NITROGEN

T_∞ °K	T_s °K	$\frac{T_\infty}{T_M}$	$\frac{\rho_\infty}{\rho_M}$	SYMBOL
1495 - 1465	361.0	1.598 - 1.604	2.204 - 2.221	×
1435 - 1465	428	1.540 - 1.548	2.073 - 2.090	⊙
1435 - 1465	495.9	1.486 1.494	1.953 - 1.972	⊡

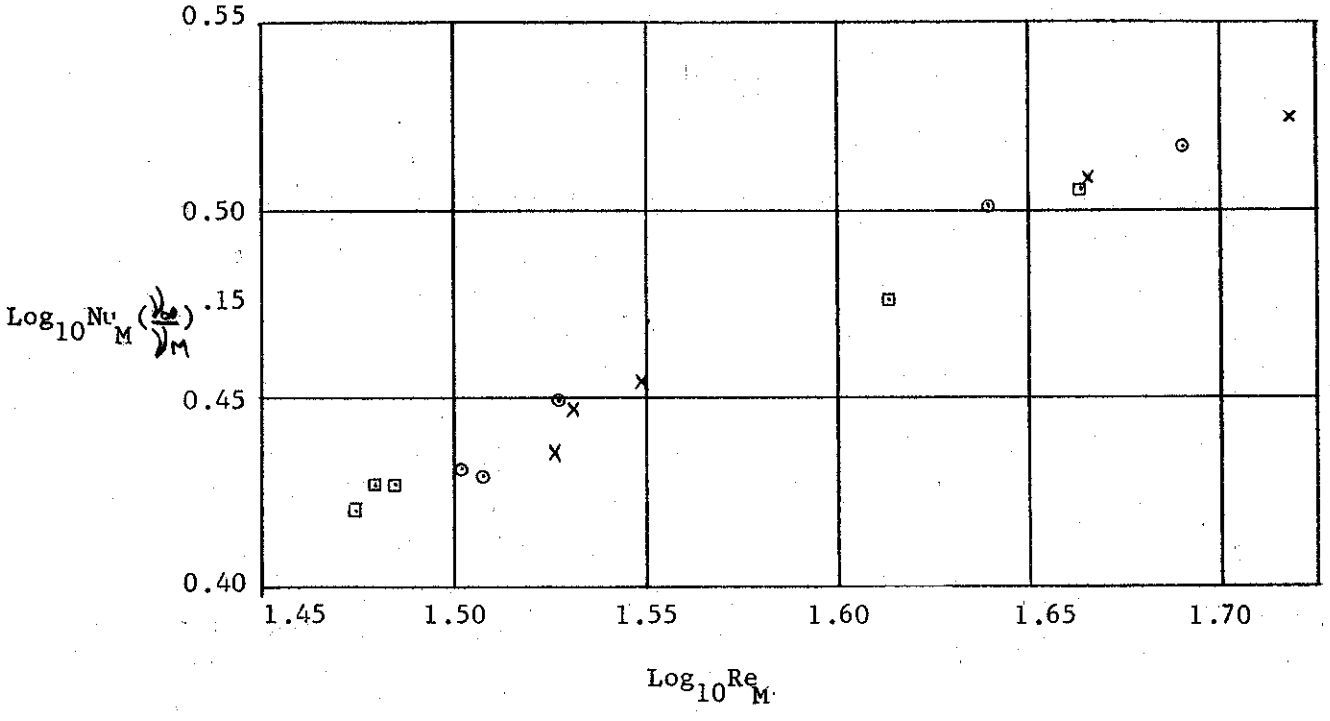

FIGURE 20B - $Nu_M(\nu_\infty/\nu_M)^{.15}$ V_s Re_M FOR NITROGEN CROSS-FLOW SHOWING ELIMINATION OF RESIDUAL TEMPERATURE LOADING EFFECT.

CYLINDER DIA. - .0152 c m.
FLOW - NITROGEN

T_∞ °K	T_s °K	$\frac{T_\infty}{T_M}$	$\frac{\nu_\infty}{\nu_M}$	SYMBOL
1495 - 1465	361.0	1.598 - 1.604	2.204 - 2.221	×
1435 1465	428	1.540 - 1.548	2.073 - 2.090	⊙
1435 - 1465	495.9	1.486 - 1.494	1.953 - 1.972	⊡

FIGURE 21A - Nu_M V_s Re_M FOR A CIRCULAR CYLINDER IN HELIUM CROSS-FLOW FOR VARIOUS TEMPERATURE LOADINGS. TEMPERATURE LOADING EFFECT OBTAINED BY VARYING T_S WHILE KEEPING T_∞ CONSTANT.

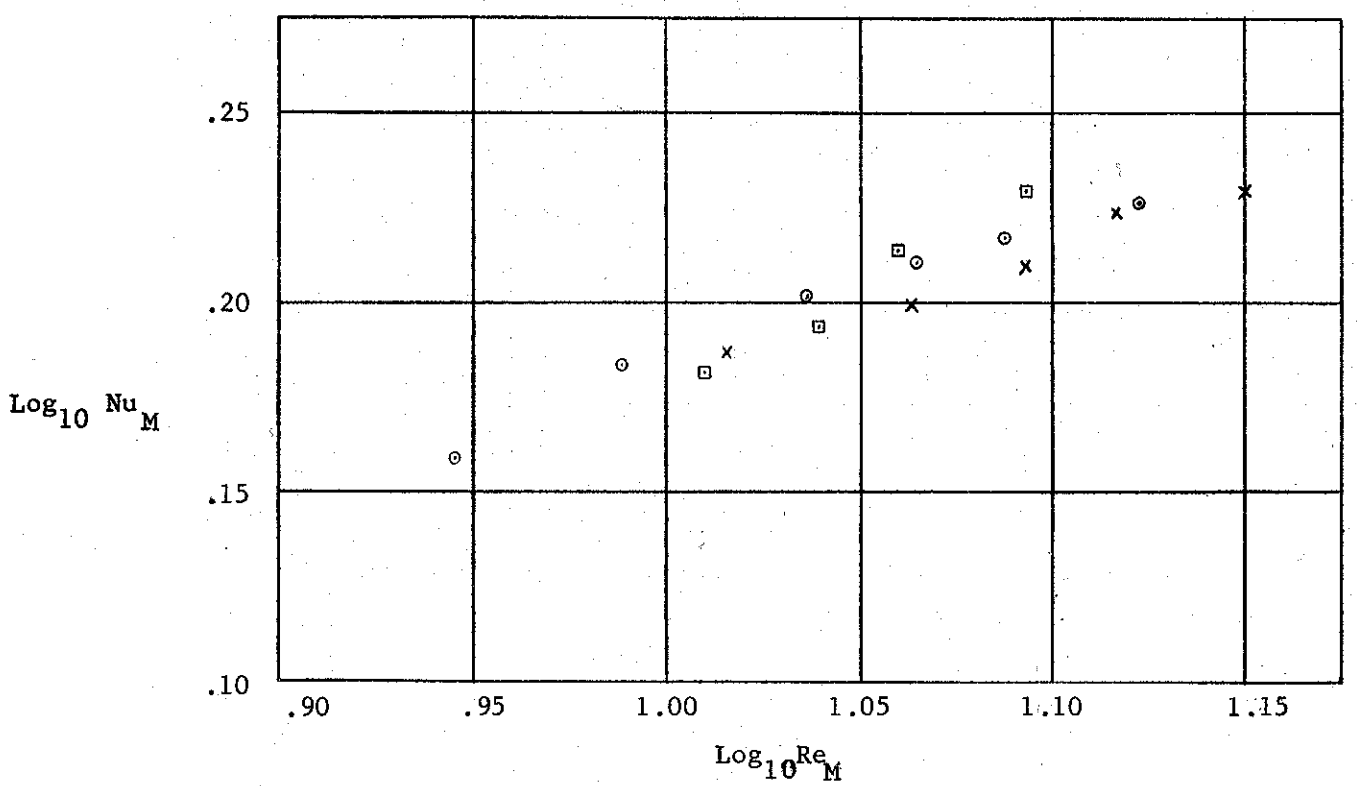

CYLINDER DIA. - .0152 c m.
FLOW - HELIUM

T_∞ °K	T_s °K	$\frac{T_\infty}{T_M}$	$\frac{\nu_\infty}{\nu_M}$	SYMBOL
1356.0 - 1360.0	387.0	1.556 - 1.557	2.044 - 2.045	×
1356.0 1360.0	460.0	1.493 - 1.494	1.910 - 1.920	⊙
1356.0 - 1360.0	532.0	1.436 - 1.437	1.792 - 1.802	⊡

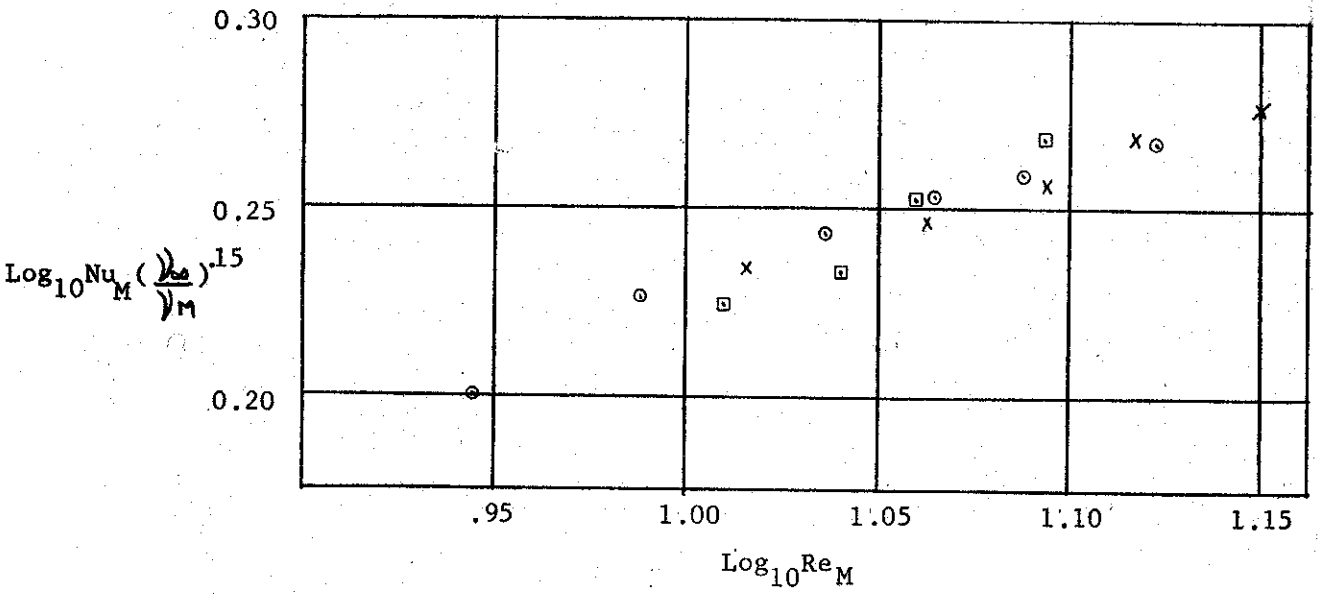

FIGURE 21B - $Nu_M (\nu_\infty/\nu_M)^{.15}$ Vs Re_M FOR HELIUM CROSS-FLOW SHOWING ELIMINATION OF RESIDUAL TEMPERATURE LOADING EFFECT.

CYLINDER DIA. - .0152 c m.
FLOW - HELIUM

T_∞ °K	T_s °K	$\frac{T_\infty}{T_M}$	$\frac{\nu_\infty}{\nu_M}$	SYMBOL
1356.0 - 1360.0	387.0	1.556 - 1.557	2.044 2.045	X
1356.0 - 1360.0	460.0	1.493 - 1.494	1.910 1.920	⊙
1356.0 - 1360	532.0	1.436 1.437	1.792 1.802	⊡

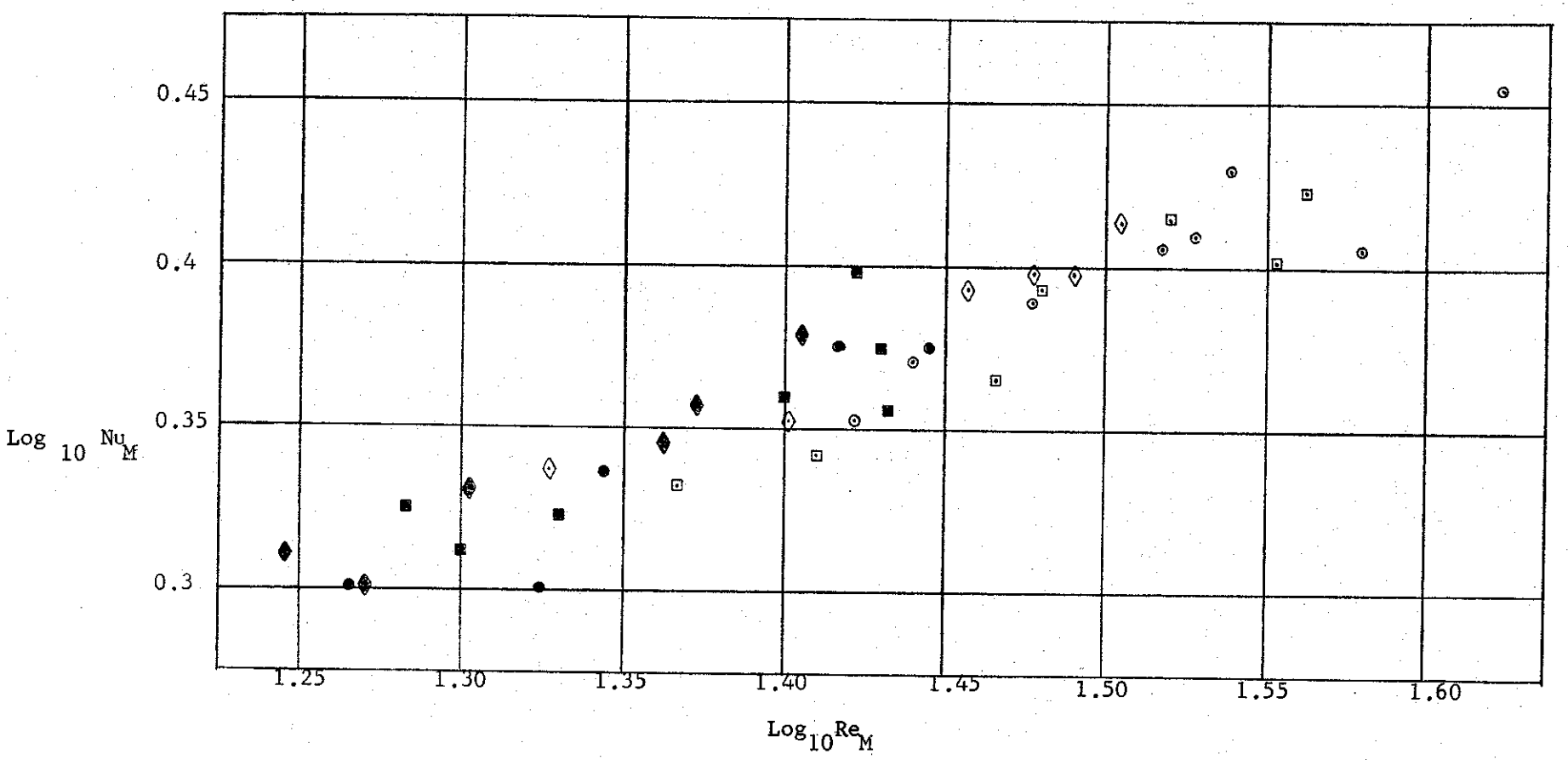

FIG.22A- Nu_M V_s Re_M FOR A CIRCULAR CYLINDER IN HELIUM-NITROGEN MIXTURE CROSS FLOW FOR VARIOUS TEMPERATURE LOADINGS. TEMPERATURE LOADING EFFECT OBTAINED BY VARYING T_∞ AND KEEPING T_s CONSTANT. Legend - See page 66.

LEGEND FOR FIGS. 22A and 22B

CYLINDER DIA. - .0152 c m.

FLOW - He-40%; N_2-60% (BY VOL)

T_∞ °K	T_s °K	$\frac{T_\infty}{T_M}$	$\frac{\nu_\infty}{\nu_M}$	SYMBOL
1266.7 - 1268.5	427.2	1.495 - 1.496	1.960 - 1.961	⊙
1088.2 - 1088.7	427.2	1.486	1.827	⊡
900.4 - 900.8	427.2	1.356	1.654	◈
FLOW - He-77.5%; N_2-22.5% (BY VOL)				
1267.3 - 1270	430.6	1.493	1.940	●
1088.3 - 1090.4	430.6	1.483	1.815	■
900.15 900.71	430.6	1.353	1.647	◆

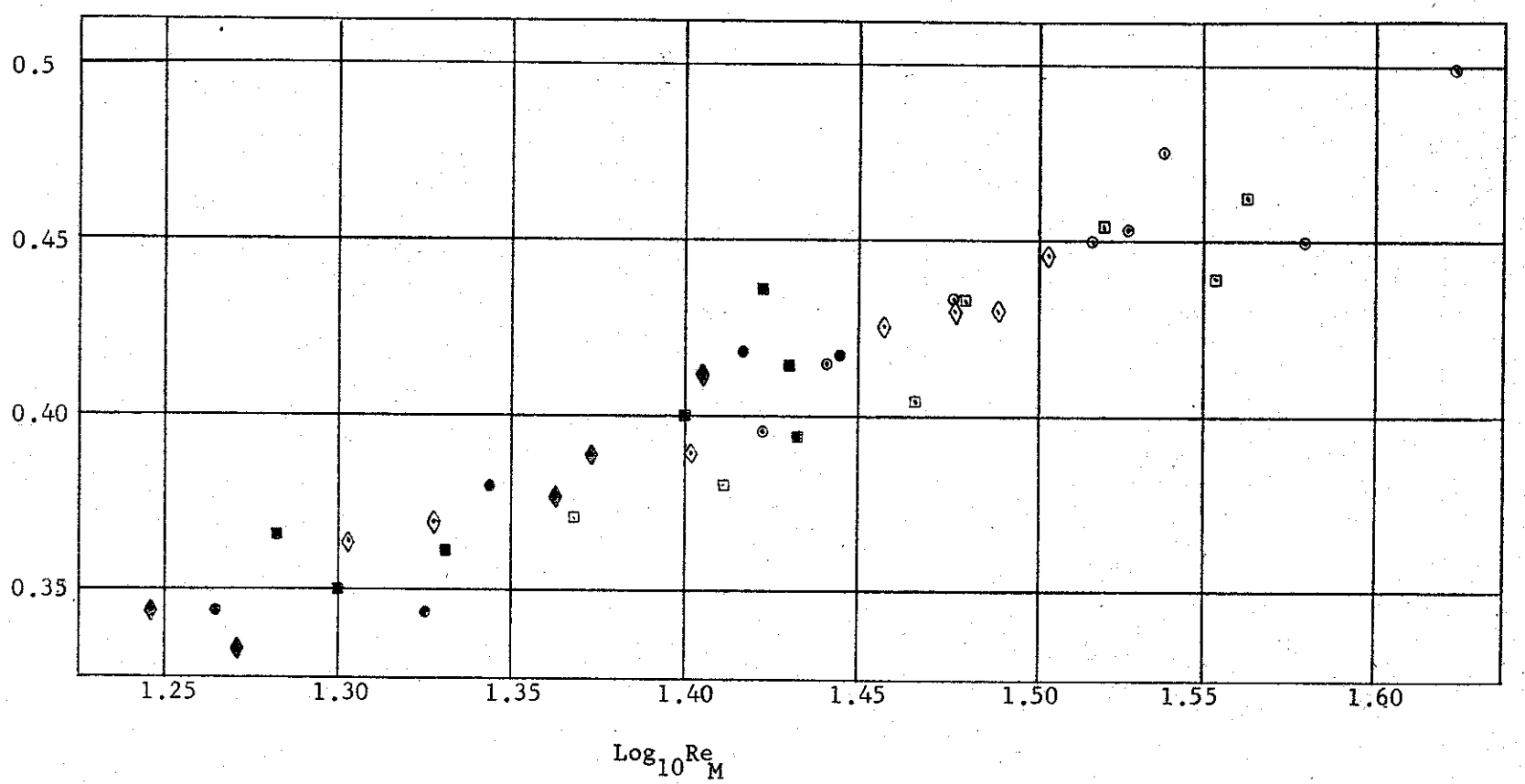

FIG. 22B- $Nu_M \left(\nu_\infty/\nu_M\right)^{.15}$ Vs Re_M FOR HELIUM-NITROGEN MIXTURE CROSS-FLOW SHOWING ELIMINATION OF RESIDUAL TEMPERATURE LOADING EFFECT

Legend - See Page 66.

FIG. 23A Nu_M Vs Re_M FOR A CIRCULAR CYLINDER IN NITROGEN CARBON DIOXIDE MIXTURE CROSS-FLOW FOR VARIOUS TEMPERATURE LOADINGS. TEMPERATURE LOADING EFFECT OBTAINED BY VARYING T_∞ AND KEEPING T_s CONSTANT.

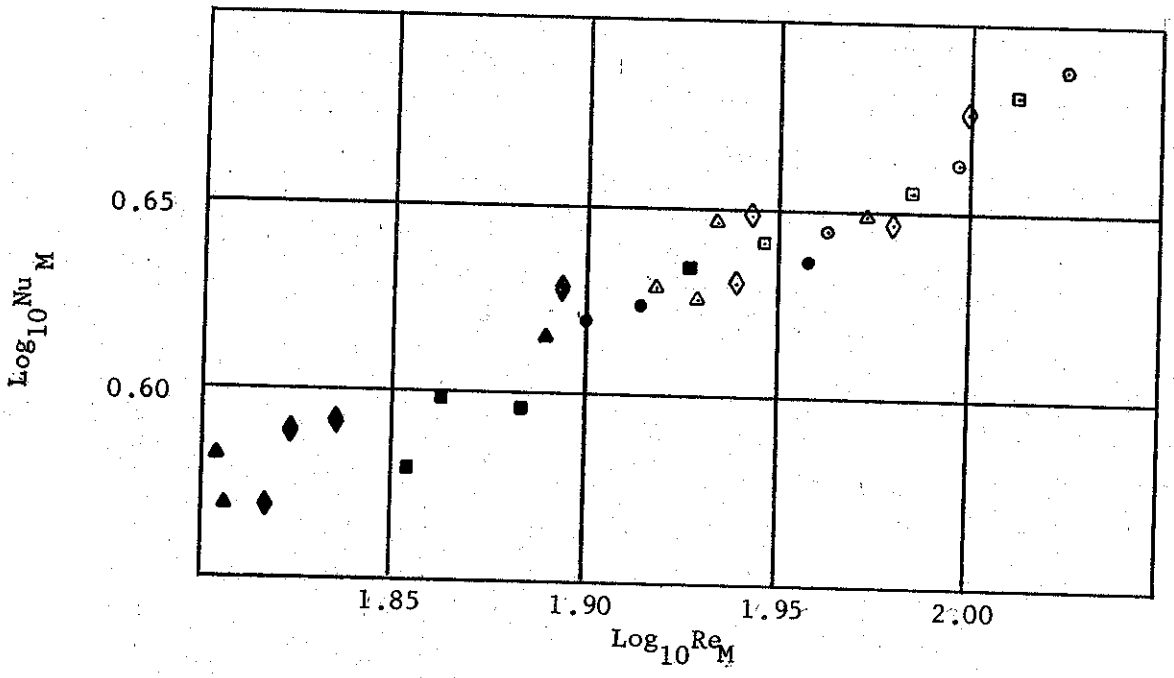

CYLINDER DIA - .0152 c m.
FLOW - N_2-30%; CO_2-70% (BY VOL)

T_∞ °K	T_s °K	$\frac{T_\infty}{T_M}$	$\frac{\nu_\infty}{\nu_M}$	Symbol
1274.8 - 1276.7	437.9	1.489	1.859	⊙
1093.1 - 1094.4	437.9	1.428	1.739	⊡
903.0 - 903.7	437.9	1.347	1.585	◇
703.2 - 703.7	437.9	1.233	1.380	△
		FLOW - N_2-50%; CO_2-50% (BY VOL)		
1276.0 - 1278.0	437.9	1.489	1.883	●
1093.8 - 1095.0	437.9	1.428	1.758	■
903.4 - 904.2	437.9	1.347	1.598	◆
703.6	437.9	1.233	1.386	▲

FIG. 23B - $Nu_M(\nu_\infty/\nu_M)$ Vs Re_M FOR NITROGEN CARBON DIOXIDE MIXTURE CROSS-FLOW SHOWING ELIMINATION OF RESIDUAL TEMPERATURE LOADING EFFECT

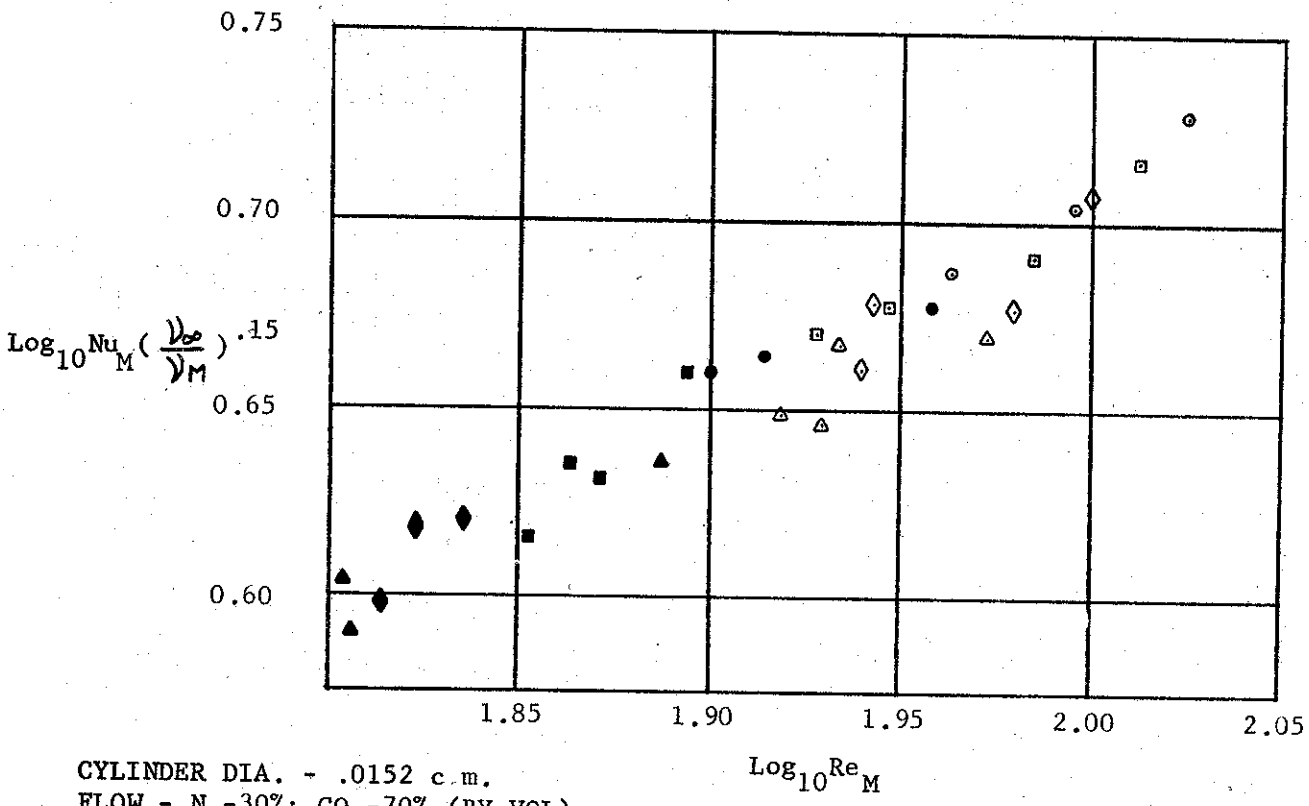

CYLINDER DIA. - .0152 c.m.

FLOW - N_2-30%; CO_2-70% (BY VOL)

T_∞ °K	T_s °K	$\frac{T_\infty}{T_M}$	$\frac{\nu_\infty}{\nu_M}$	SYMBOL
1274.8 - 1276.7	437.9	1.489	1.859	⊙
1093.1 - 1094.4	437.9	1.428	1.739	⊡
903.0 - 903.7	437.9	1.347	1.585	◇
703.2 - 703.7	437.9	1.233	1.380	△

FLOW - N_2-50%; CO_2-50% (BY VOL)

1276.0 - 1278.0	437.9	1.489	1.883	●
1093.8 - 1095.0	437.9	1.428	1.758	■
903.4 - 904.2	437.9	1.347	1.598	◆
703.6	437.9	1.233	1.386	▲

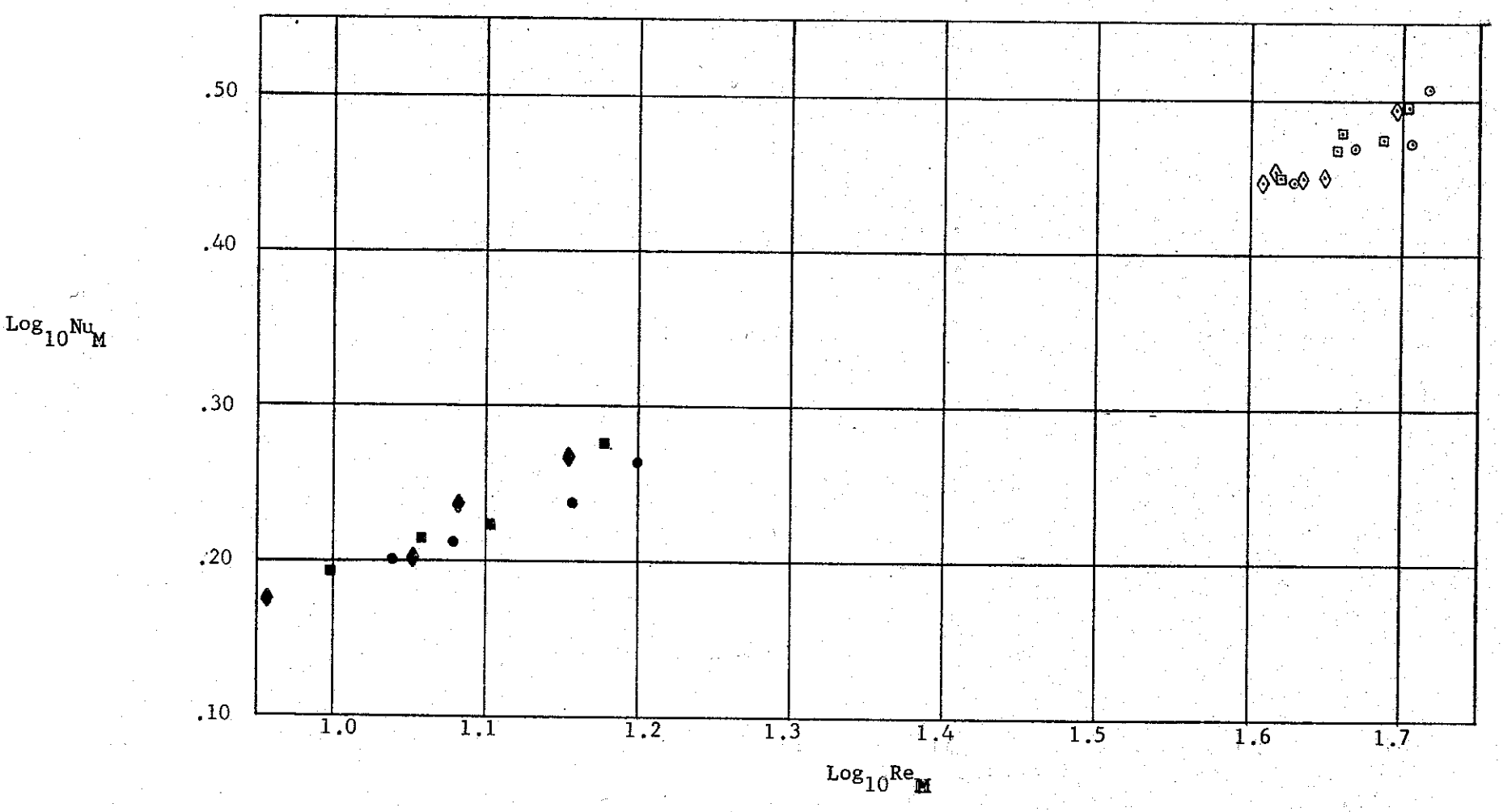

FIG. 24A - Nu_M V_s Re_M FOR A CIRCULAR CYLINDER IN HELIUM CARBON DIOXIDE MIXTURE CROSS-FLOW FOR VARIOUS TEMPERATURE LOADINGS. TEMPERATURE LOADING EFFECT OBTAINED BY VARYING T_∞ AND KEEPING T_S CONSTANT. Legend - see page 71.

LEGEND FOR FIGS. 24A and 24B

CYLINDER DIA. - .0152 c m.

FLOW - He-42%; CO_2-58% (BY VOL)

T_∞ ^oK	T_s ^oK	$\frac{T_\infty}{T_M}$	$\frac{\nu_\infty}{\nu_M}$	SYMBOL
1087.5 - 1088.2	368.13	1.4943	1.899	⊙
899.85 - 900.28	368.13	1.4194	1.743	⊡
701.82 - 702.14	368.13	1.3456	1.533	◇
FLOW - He-93.5%; CO_2-6.5%				
1088.5 - 1089.4	368.13		1.928	●
900.6 - 900.94	368.13		1.773	■
702.06 - 702.47	368.13		1.555	◆

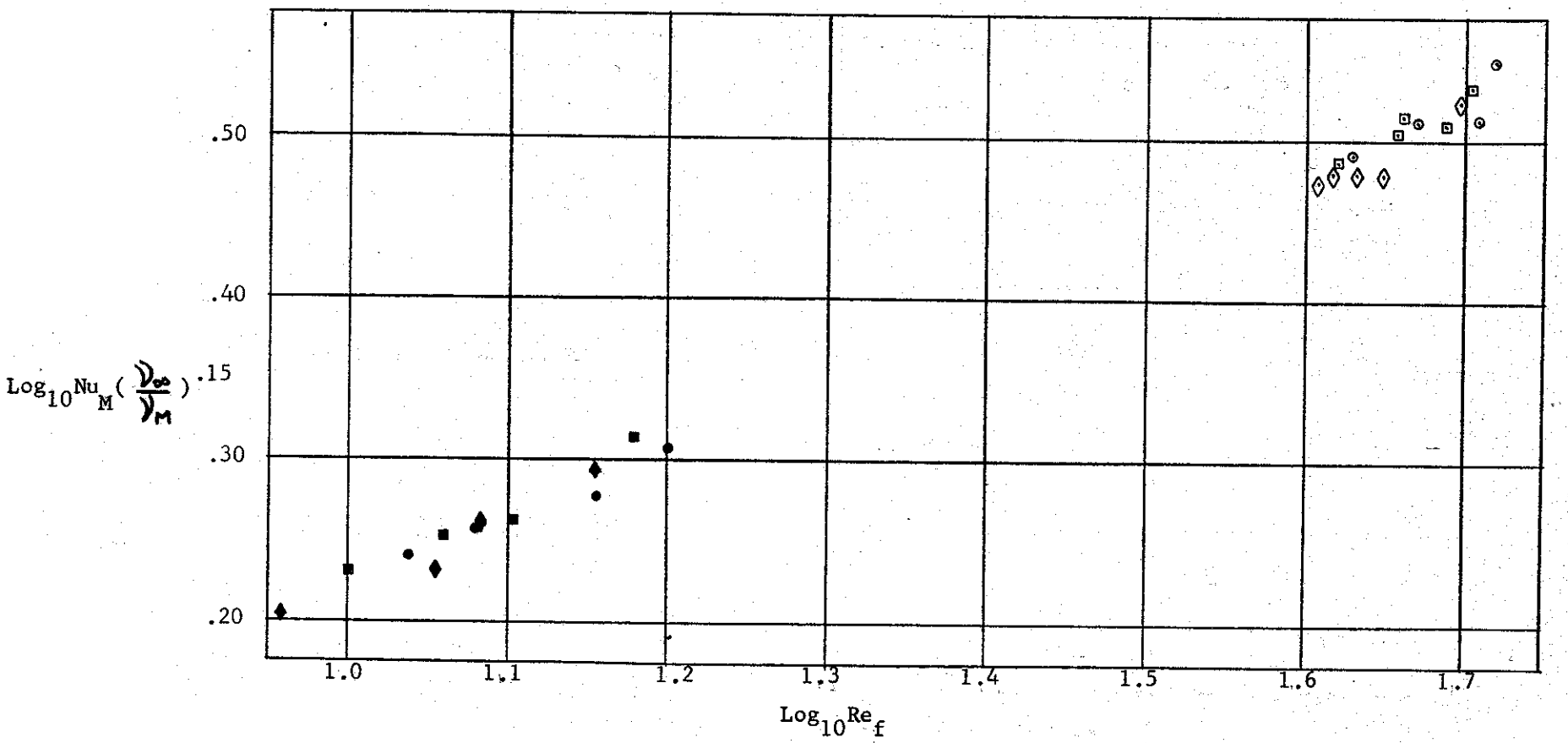

FIG. 24B - $Nu_M(\nu_\infty/\nu_M)^{.15}$ V_s Re_M FOR HELIUM CARBON DIOXIDE MIXTURE CROSS FLOW SHOWING ELIMINATION OF RESIDUAL TEMPERATURE LOADING EFFECT. Legend see page 71.

FIG. 25 - $Nu_M \left(\frac{\nu_\infty}{\nu_M}\right)^{.15}$ V_S Re_M FOR A CIRCULAR CYLINDER IN CROSS FLOW OF VARIOUS SPECIES AND SPECIE MIXTURES. Legend - see page 74.

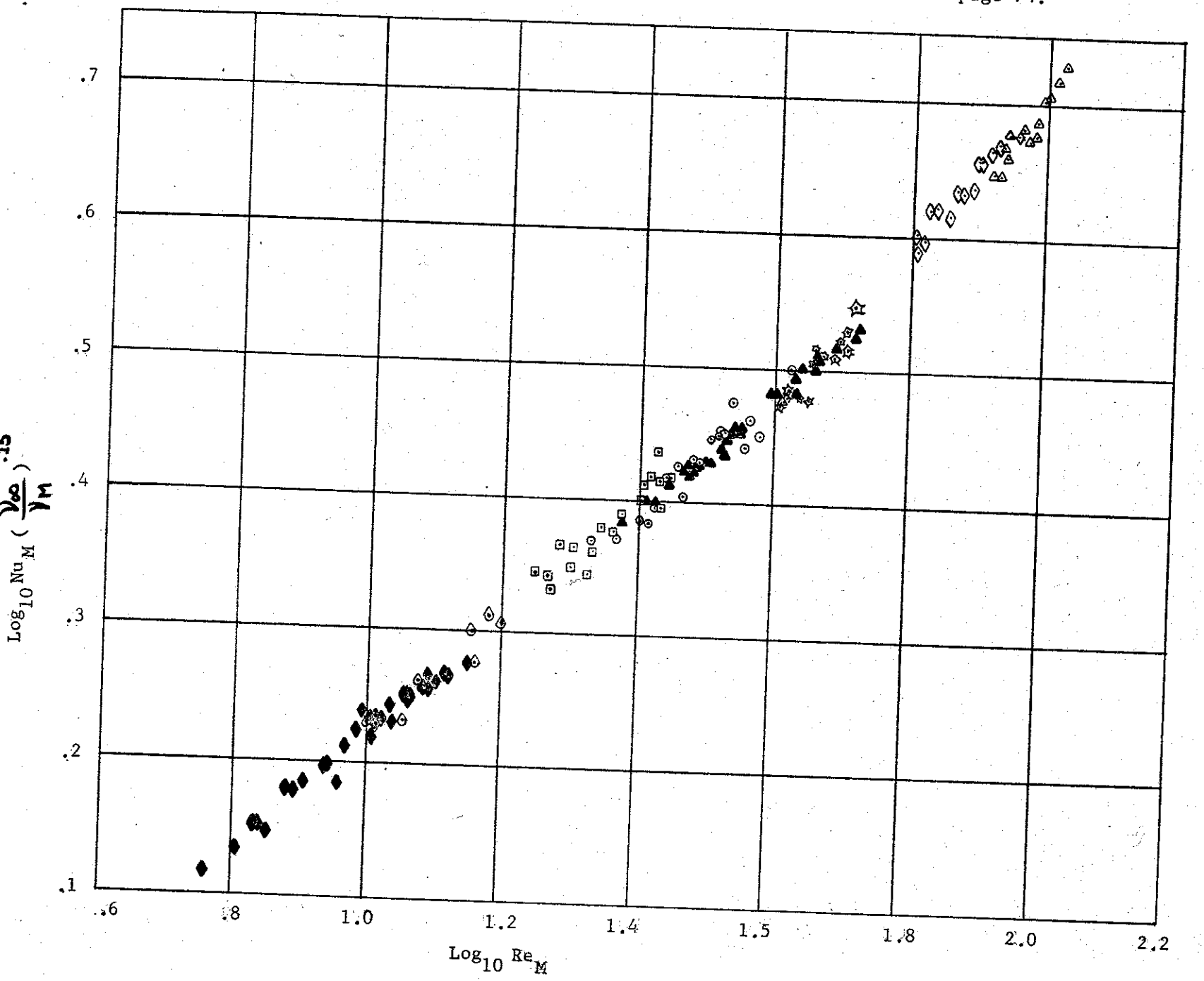

LEGEND FOR FIGS. 25 and 26

CYLINDER DIA. - .0152 c.m.

Specie or specie mixture by vol.	T_∞ °K	T_s °K	$\frac{T_\infty}{T_M}$	$\frac{\nu_\infty}{\nu_M}$	Symbol
NITROGEN	See Figs. 18A or 18B and 20A or 20B				▲
HELIUM	See Figs. 19A or 19B and 21A or 21B				♦
He-40% - N_2-60%	See Figs. 22A or 22B				⊙
He-77.5% - N_2-22.5%	See Figs. 22A or 22B				⊡
N_2-50% CO_2-50%	See Figs. 23A or 23B				◈
N_2-30% CO_2-70%	See Figs. 23A or 23B				◬
He-42% CO_2-58%	See Figs. 24A or 24B				☆
He-93.5% CO_2-6.5%	See Figs. 24A or 24B				⊙

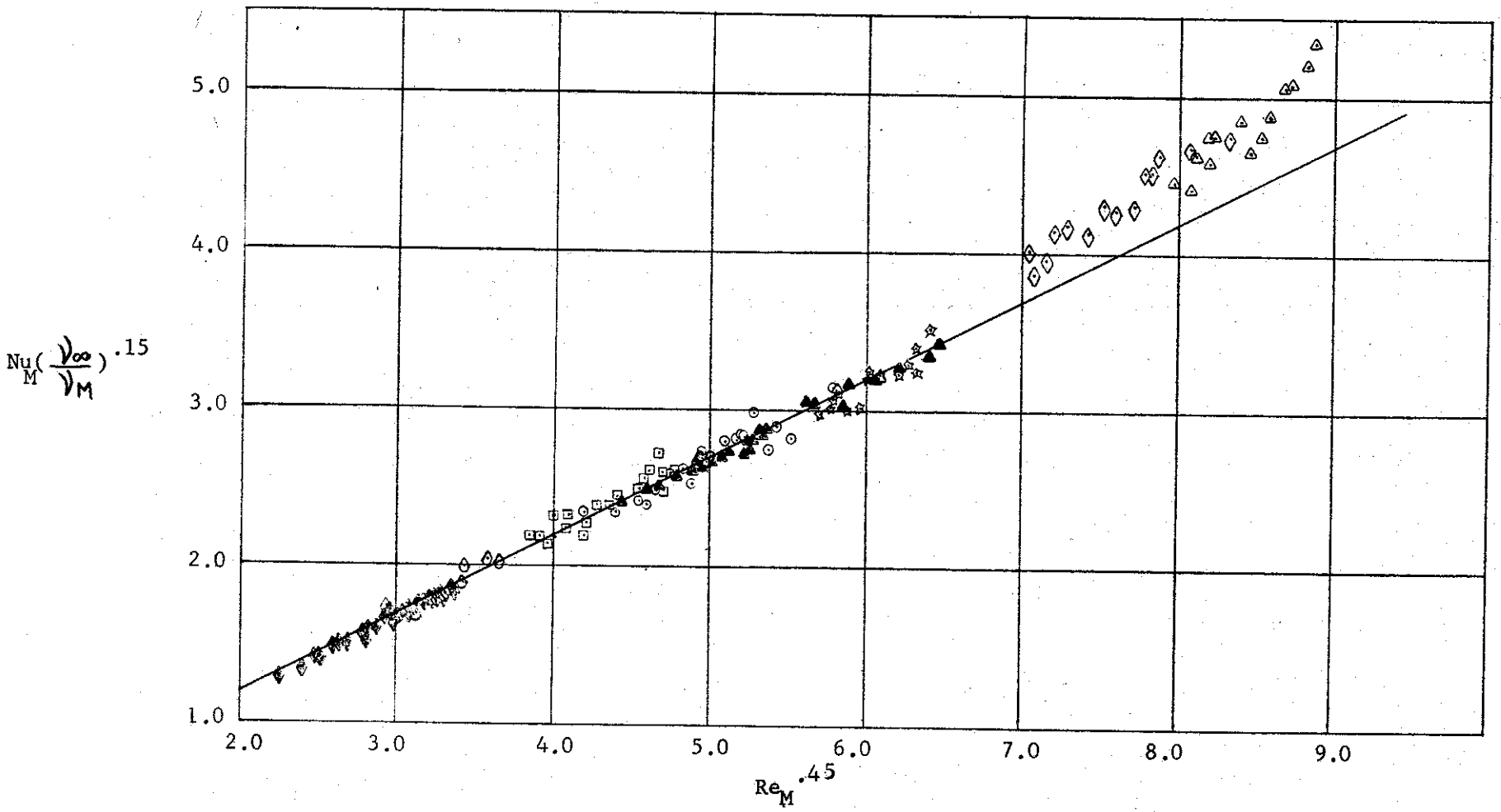

FIG.26- $Nu_M\ (\nu_\infty/\nu_M)^{.15}$ Vs $Re_M^{.45}$ SHOWING ALL HEAT TRANSFER DATA FOR VARIOUS SPECIES AND SPECIE MIXTURES AND FOR VARIOUS TEMPERATURE LOADINGS UNIQUELY CORRELATED BY THE RELATION $Nu_M(\nu_\infty/\nu_M)^{.15} = .2068 + .4966\ Re_M^{.45}$ IN THE Re_M RANGE OF 5 TO 40. Legend - see page 74.

FIG. 27 - COMPARISON OF PRESENT CORRELATION FOR FORCED CONVECTIVE HEAT TRANSFER TO COOLED CYLINDERS IN HEATED CROSS-FLOW WITH PREVIOUS CORRELATIONS FOR HEAT TRANSFER FROM HEATED CYLINDERS IN AMBIENT OR NEAR-AMBIENT CROSS-FLOW.

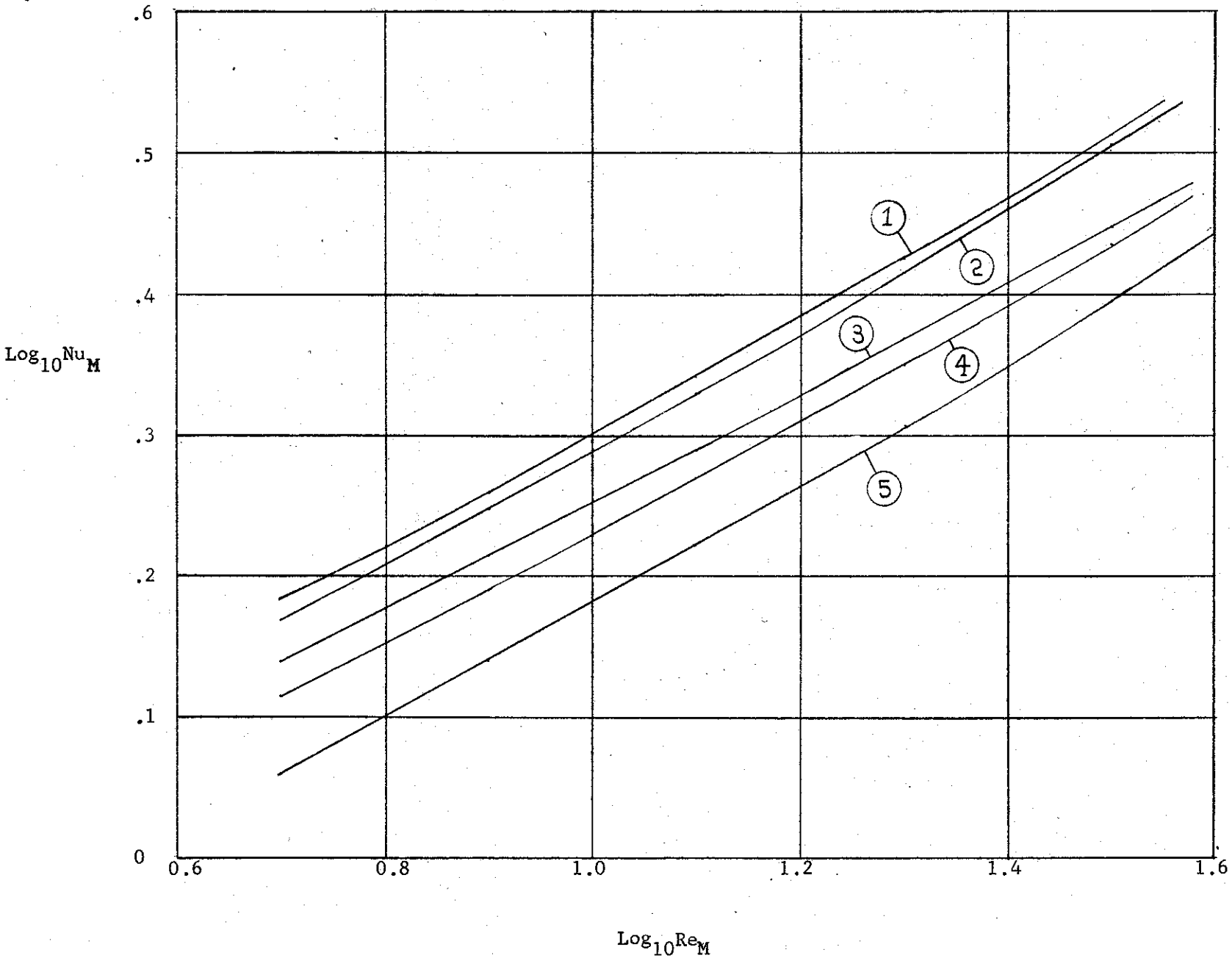

Legend - see page 77

LEGEND FOR FIG. 27

1. KRAMER : $Nu_M = 0.42Pr_M^{0.20} + 0.57Pr_M^{0.33}Re_M^{0.50}$

2. VAN DER HEGGE ZIJNEN : $Nu_M = 0.35 + 0.5Re_M^{0.5} + .001Re_M$

3. COLLIS AND WILLIAMS : $Nu_M = (0.24 + 0.56Re_M^{0.45})\left(\frac{T_M}{T_\infty}\right)^{.17}$

4. HILPERT : $Nu_M = .821\left(Re_M(T_S/T_\infty)^{.25}\right)^{.385}$

5. PRESENT RESULT : $Nu_M = (0.2068 + .4966Re_M^{0.45})\left(\frac{\mu_\infty}{\mu_M}\right)^{-.15}$

CONDITIONS OF COMPARISON:

T_S = $400^\circ K$

T_∞ = $1200^\circ K$

FLOW = NITROGEN

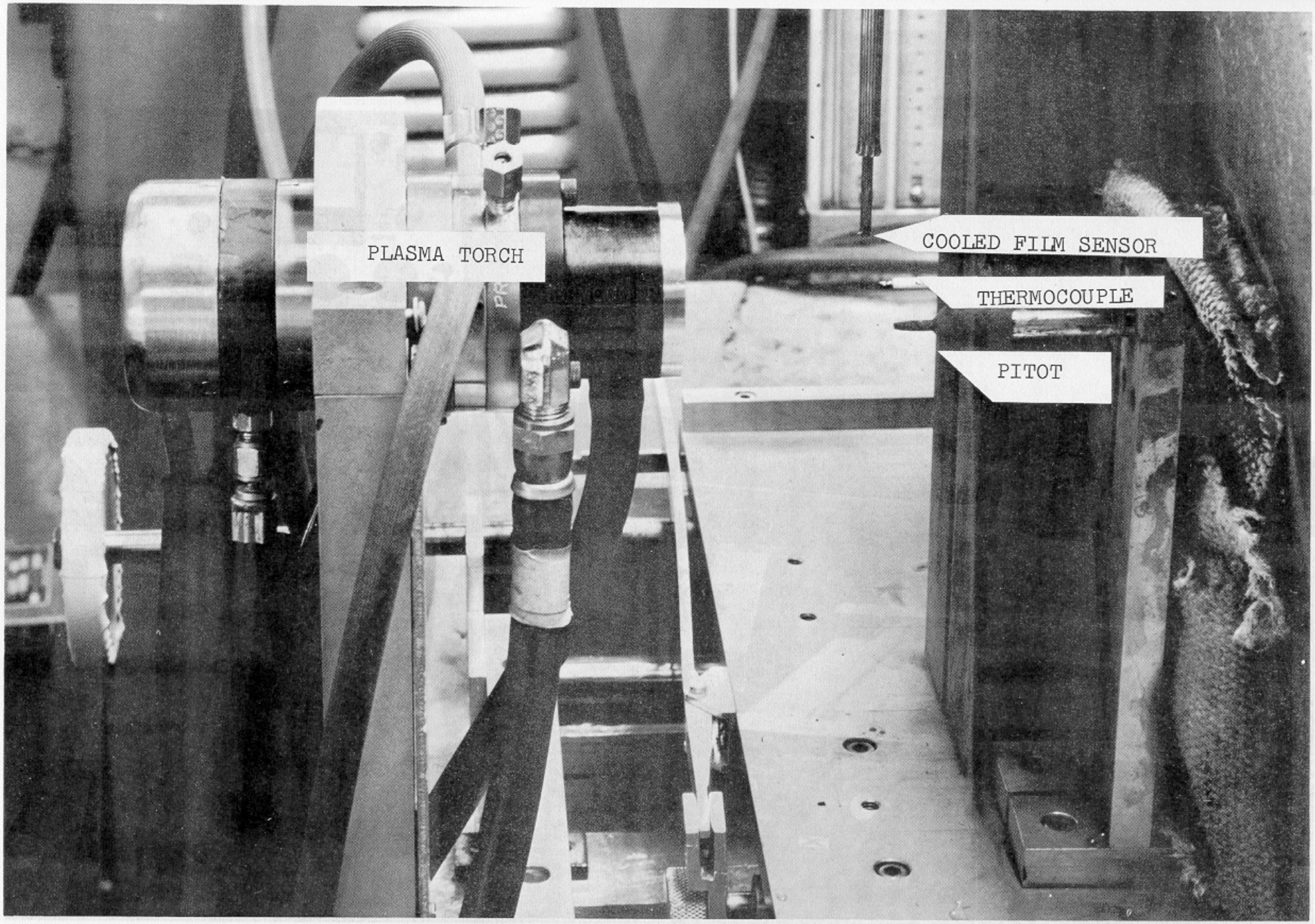

FIG. 12 - CLOSE UP VIEW OF PLASMA TORCH AND INSTRUMENTS